Generalized Rapid-distortion theory on transversely sheared mean flows with physically realizable upstream boundary conditions: Application to trailing edge problem

M. E. Goldstein[1], S. J. Leib[2] & M. Z. Afsar[3]

[1]National Aeronautics and Space Administration, Glenn Research Centre, Cleveland OH 44135, USA

[2]Ohio Aerospace Institute, Cleveland, OH 44142 USA

[3]Strathclyde University, Department of Mechanical and Aerospace Engineering, 75 Montrose St. Glasgow, GI 1XJ

This paper is concerned with rapid distortion theory on transversely sheared mean flows which (among other things) can be used to analyze the unsteady motion resulting from the interaction of a turbulent shear flow with a solid surface. It extends previous analyses of Goldstein, Afsar & Leib (2013 a, b) which showed that the unsteady motion is completely determined by specifying two arbitrary convected quantities. The present paper uses a pair of previously derived conservation laws to derive upstream boundary conditions that relate these quantities to experimentally measurable flow variables. The result is dependent on the imposition of causality on an intermediate variable that appears in the conservation laws. Goldstein et al (2013a) related the convected quantities to the physical flow variables at the location of the interaction, but the results were not generic and hard to reconcile with experiment. That problem does not occur in the present formulation which leads to a much simpler and more natural result than the one given in Goldstein et al (2013a). We also show that the present formalism yields better predictions of the sound radiation produced by the interaction of a two-dimensional jet with the downstream edge of a flat plate than the Goldstein et al (2013a) result. The role of causality is also discussed.

---

1. Introduction

Rapid Distortion Theory (RDT) uses linear analysis to study the interaction of turbulence with solid surfaces. It applies whenever the turbulence intensity is small and the length (or time) scale over which the interaction takes place is short compared to the length (or time) scale over which the turbulent eddies evolve (Hunt, 1973; Goldstein, 1978a,1979a). When interpreted asymptotically, these assumptions imply, among other things, that it is possible to identify a distance that is very (infinitely) large on the scale of the interaction, but still small on the scale over which the turbulent eddies evolve. The assumptions also imply that the resulting flow is inviscid and non-heat conducting and is, therefore, governed by the Linearized Euler Equations, i.e., the Euler equations linearized about an arbitrary, usually steady, solution to the nonlinear equations— customarily referred to as the base flow.

The simplest case occurs when the base flow is completely uniform. In his now classical paper, Kovasznay (1953) showed that the unsteady isentropic motion on this flow can be decomposed into the sum of a vortical disturbance that has no pressure fluctuations and an irrotational disturbance that carries the pressure fluctuations. The latter satisfies a second-order wave equation when the flow is compressible and should either decay or propagate relative to the base flow. It can, therefore be associated with the acoustic component of the motion on these flows. The former, which moves downstream at the mean flow velocity, i.e., it is a purely convected quantity, can be associated with the remaining, hydrodynamic, component of the motion. Any convected velocity field will satisfy the linearized momentum equations for this flow, but continuity only allows two of its components to be arbitrary. These two quantities can then be independently specified as time stationary boundary conditions for unsteady surface interaction problems. This makes the Kovasznay decomposition particularly useful for analyzing problems that involve the interaction of turbulence (which corresponds to the hydrodynamic component of the motion) with surfaces embedded in uniform mean flows (Sears, 1941), or in flows that become uniform in the upstream region (Hunt, 1973; Goldstein, 1978a, 1979a,). It is worth noting, however, that the Kovasznay decomposition is not unique because there are irrotational (homogeneous) solutions that carry no pressure fluctuations and can therefore be associated with either the vortical component or with the irrotational component.

There have been a number of attempts to extend these ideas to non-uniform base flows, but the situation is considerably more complicated when the entire base flow is non-uniform. The simplest case occurs when the base flow U is incompressible and the mean shear is uniform, i.e.

$$U = \gamma y_2, \tag{1.1}$$

where γ is a constant and y_1, y_2, y_3 are Cartesian coordinates, with y_1 being in the mean flow direction. Then the two-dimensional small-amplitude motion is determined by the linearized incompressible vorticity equation, $\left(\partial / \partial\tau + U\partial / \partial y_1\right)\omega_3' = 0,$ where τ denotes the time and ω_3' the two-dimensional spanwise vorticity perturbation. Orr (1907, see also Drazin & Reid, 1981, pp. 147-151) pointed out that this equation or, equivalently, the two-dimensional Rayleigh equation

$$\frac{\partial}{\partial y_1}\left(\frac{\partial}{\partial\tau} + U\frac{\partial}{\partial y_1}\right)\omega_3' = \left(\frac{\partial}{\partial\tau} + U\frac{\partial}{\partial y_1}\right)\left(\frac{\partial^2}{\partial y_1^2} + \frac{\partial^2}{\partial y_2^2}\right)v_2' = 0, \tag{1.2}$$

which determines the unsteady cross-gradient velocity perturbation $v_2'\left(y_2, \tau\right)$ can be integrated to obtain

$$\left(\frac{\partial^2}{\partial y_1^2} + \frac{\partial^2}{\partial y_2^2}\right)v_2' = \frac{\partial}{\partial y_1}\omega_c\left(\tau - \frac{y_1}{\gamma y_2}, y_2\right), \tag{1.3}$$

where the imposed spanwise vorticity perturbation ω_3', which we denote by ω_c, can be an arbitrary function of its arguments. Orr (1907) obtained an analytic solution to an initial value problem associated with this equation and used it to study the development of the velocity and pressure fluctuations starting from some initial state. But the long-time solutions to at least some initial value problems are likely to develop internal shear layers that can no longer be considered inviscid and are susceptible to Kelvin-Helmholtz instabilities (Brinkman & Walker, 2001; Cowley, 2001; Cassel & Conlisk, 2014) and are therefore not necessarily relevant to the time-stationary turbulent flows being considered here. It does, however, seem reasonable to use the steady state (i.e., time-stationary) solutions of this equation to represent the turbulence in these flows. The solutions will then be of the form

$$v_2'\left(\boldsymbol{x}, t\right) = \frac{\partial}{\partial x_1}\int_{-T}^{T}\int g_0\left(\boldsymbol{x}, t \mid \boldsymbol{y}, \tau\right)\omega_c\left(\tau - \frac{y_1}{\gamma y_2}, y_2\right)d\boldsymbol{y}d\tau, \tag{1.4}$$

where $\boldsymbol{x} = \left\{x_1, x_2\right\}$, $\boldsymbol{y} = \left\{y_1, y_2\right\}$ denote the two-dimensional Cartesian coordinates, T denotes a large time interval and g_0 is a two-dimensional Green's function that satisfies the Poisson equation

$$\left(\frac{\partial^2}{\partial x_1^2}+\frac{\partial^2}{\partial x_2^2}\right)g_0\left(\boldsymbol{x},t\,|\,\boldsymbol{y},\tau\right)=\delta\left(t-\tau\right)\delta\left(\boldsymbol{y}-\boldsymbol{x}\right) \tag{1.5}$$

The vorticity ω_3', which is equal to the convected quantity $\omega_c\left(\tau-y_1/U\left(y_2\right),y_2\right)$, can now be specified as a boundary condition since(1.4) will satisfy (1.3) for any choice of this quantity. The inner integral in (1.4) will be over a bounded or semi-bounded region of space, with the Green's function g_0 chosen to satisfy appropriate transverse boundary conditions when solid surfaces are present in the flow and the integral will the integral will be over all space and g_0 can therefore be taken to be $\left(4\pi\right)^{-1}\ln\left|\boldsymbol{x}-\boldsymbol{y}\right|^2\delta\left(t-\tau\right)$ when they are not. The transverse velocity perturbation $v_2'\left(\boldsymbol{x},t\right)$ would then be given by (see Gradshteyn & Ryzhik p.406 #3.723)

$$v_2'\left(\boldsymbol{x},t\right)=\int_{-\infty}^{\infty}\bar{G}_0\left(x_2\left|y_2\right.\right)\omega_c\left(t-x_1/\gamma y_2\right)dy_2 \tag{1.6}$$

with

$$\bar{G}_0\left(x_2\left|y_2\right.\right)\equiv\frac{i}{2}(\operatorname{sgn}\omega)(\operatorname{sgn}y_2)e^{-|\omega||x_2-y_2|/\gamma|y_2|} \tag{1.7}$$

when the convected vorticity $\omega_c\left(\tau-y_1/U\left(y_2\right),y_2\right)$ is taken to be the generic time-harmonic function

$$\omega_c\left(t-\frac{y_1}{U\left(y_2\right)},y_2\right)=e^{i\omega\left[t-y_1/U\left(y_2\right)\right]}\tilde{\Omega}_c\left(y_2:\omega\right) \tag{1.8}$$

which can be summed over frequency to represent an arbitrary-time dependent flow. Some typical results for the transverse velocity perturbation resulting from (1.8) with $\tilde{\Omega}_c\left(y_2:\omega\right)$ taken to be

$$\tilde{\Omega}_c\left(y_2:\omega\right)=e^{-\left[a\left(y_2-y_0\right)\right]^2} \tag{1.9}$$

are plotted in figure 1, which shows that this quantity differs from its purely convected counterpart on a uniform mean flow in that it now decays as $x_1\to\pm\infty$.

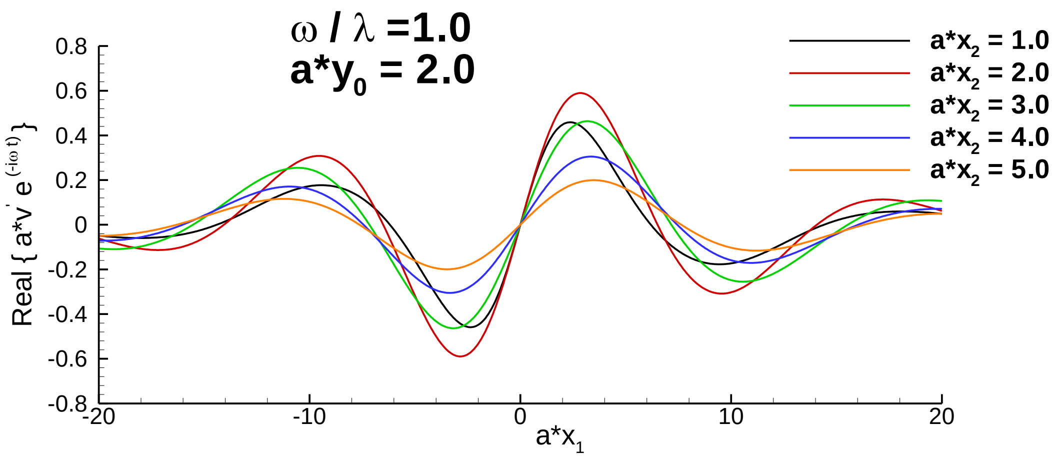

(a) Real part

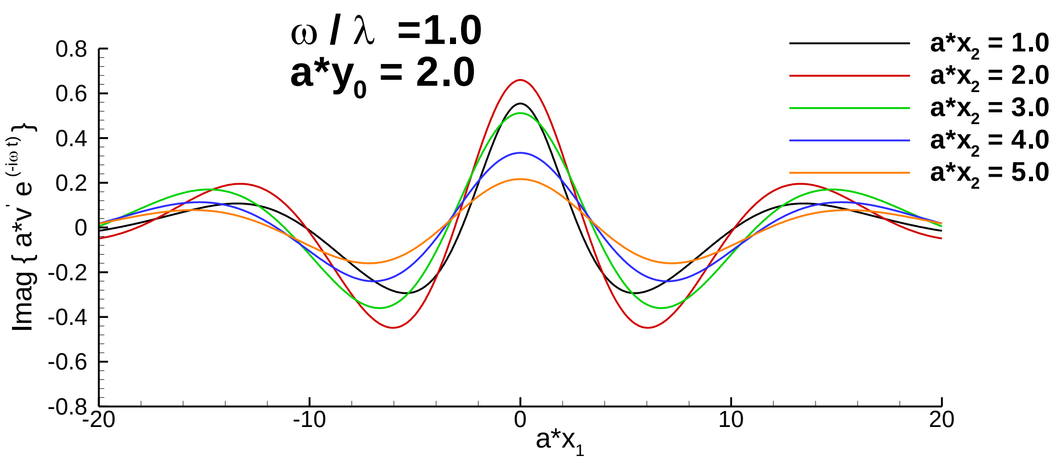

(b) Imaginary part

Figure 1 Transverse velocity fluctuations produced by the convected vorticity(1.8) for the indicated values of the parameters.

Similar behavior is also expected to occur in surface interaction problems, which might, for example, involve placing a leading edge at $y_1 = 0$ (see figure 2). This implies that the upstream boundary conditions cannot be imposed by simply specifying v_2' at upstream infinity when constructing solutions to these types of problems.

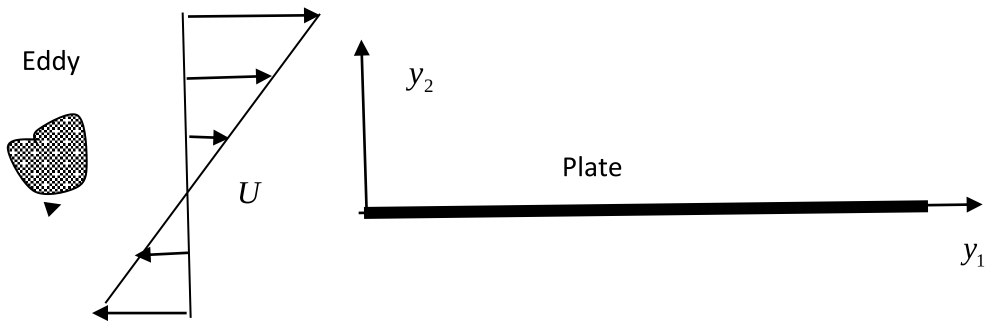

Figure 2. Leading edge scattering

But equation(1.3) shows that the Laplacian of the transverse velocity v_2' is equal to the streamwise derivative of the convected quantity $\omega_c\left(\tau-y_1/U\left(y_2\right),y_2\right)$ and, therefore does not decay, which means that it can be specified infinitely far upstream on the length scale over which the interaction takes place, which, as noted above, can be still asymptotically small compared to the scale over which the turbulent eddies evolve. The important point is that the arbitrary convected quantity $\omega_c\left(\tau-y_1/U\left(y_2\right),y_2\right)$ can be determined by specifying an appropriate experimentally measurable quantity in a region of the flow that is uninfluenced by the rapid distortion interaction. Not surprisingly, the situation is somewhat more complex for arbitrary transversely sheared mean flows which is further complicated by the need to consider causality. The focus of this paper is on extending these ideas to such flows and using the results to specify appropriate upstream boundary conditions for RDT problems on these more general mean flows.

Equation(1.3) was extended to three-dimensional compressible motions on general transversely sheared mean flows by Goldstein (1978b), Goldstein (1979b) (hereafter referred to as G78 and G79, respectively) and Goldstein, Afsar and Leib, (2013a) (hereafter referred to as GAL)--who showed how their more general results can be used to formulate RDT problems that are relevant to aircraft noise prediction. Their results can be thought of as a natural generalization of the Kovasznay (1953) decomposition in that the general formalism developed in those references, which is summarized in Section 2 of the current paper, shows that the bounded solutions to the linearized Euler equations governing the small-amplitude motion on a transversely sheared mean flow involve two purely convected quantities that can be arbitrarily specified as input conditions. But these quantities must be related to physically measurable flow variables in order to obtain solutions that can be compared with experiment. GAL obtained the required relations by assuming that they would be the same as those that would exist at the location of the scattering inhomogeneity in a streamwise-homogeneous flow (that would exist in the absence of any scattering inhomogeneities in the streamwise direction). The result was quite complicated (and ultimately had to be approximated) and, more importantly, required that the physical variables be measured in a different flow from the one being analyzed. As noted above, a major purpose of the present paper is to relate the convected quantities to the physical variables in a way that does not exhibit any of these drawbacks by imposing appropriate upstream boundary conditions in the undisturbed region of the flow being analyzed—as was done in G78 and G79. The present paper generalizes and extends these results and shows by example that this leads to considerably improved agreement with experiment.

There are a large number of papers (e.g.Taylor,1935; Batchelor and Proudman,1954; Xie, Karimi and Grimaji, 2017; Livescu and Mania, 2004; Sagaut and Cambon, 2008 and references therein) that use locally homogeneous RDT (which is a kind of local high frequency approximation) first introduced by Moffatt (1967) to study the unsteady motion on planer sheared flows (see Moffatt, 1967) . But the local nature of this approximation obviates the need to consider the upstream boundary condition issue, which is arguably the main focus of this paper. More general global solutions can be obtained by using Non-homogeneous RDT, which usually provides a more realistic representation of the turbulence but requires the imposition of upstream boundary conditions. Hunt (1973) used non-homogeneous RDT to study the distortion of turbulence by an irrotational base flow.

Early work on RDT was restricted to incompressible flows. Goldstein (1978a) and G79 introduced compressibility effects into the (more general non-homogenous) theory, which allowed the inclusion of an acoustic as well as a vortical component of the motion (as in the Kovasznay, 1953 decomposition) and not just a vortical component. But more importantly, the inclusion of compressibility enabled the application of RDT to the prediction of the radiated sound field produced by the flow. GAL used the compressible theory developed in G79 to predict the sound radiation produced by the interaction of a two-dimensional jet with the downstream edge of a flat plate. They employed low-frequency asymptotics to obtain a relatively simple explicit formula and used it to predict the radiated sound field. The results were in reasonable agreement with data but the high frequency roll off of the predicted spectrum tended to be much slower than the experimental results. The present paper shows that this deficiency can be corrected by considering the high frequency limit. We again obtain an explicit formula for the radiated sound field that reduces to the GAL result when one of its factors is set equal to unity. But this factor also approaches unity when the appropriately scaled frequency parameter approaches zero so that the result behaves like a uniformly valid composite solution that applies at all frequencies. The predictions based on this formula are found to be in much better agreement with the experiments than those given in GAL.

While GAL and the present paper use the same application to illustrate the general formalism developed (i.e., the interaction of a two-dimensional jet with the downstream edge of a flat plate) the improved relations between the theoretical convected quantities and the measureable flow variables makes the present results applicable to a wide range of flow-surface interaction problems. Examples include analysis of more complicated geometries, such as deformable plates inclined to the mean flow (Chinaud, et al, 2014), which could be of interest in optimisation studies for reducing edge-generated noise.

Linear theories are also used to study the shock-turbulence interaction and are often refered to as Linear Interaction Approximations (LIA) in this context (see for example, Ribner, 1953; Moore, 1954: Woushuk *et al*. (2009) and (2012); Huete et al. (2011) and (2012) as well as extensive discussion of the subject by Saguat & Cambon (2008)). Compressible RDT and LIA share some common features (Haute Ruiz de Lira, 2010; Haute et al, 2011 Haute, 2012 and others). Both approaches decompose the flow into acoustic and vortical components and both use Fourier and/or Laplace transforms to eliminate the time dependence.

The paper begins by briefly summarizing the results obtained in GAL for the formal solution to the complete inhomogeneous RDT problem. As in G78 & G79 the unsteady motion is determined by two convected quantities that can be arbitrarily specified as boundary (or initial) conditions. But, as noted above, it is necessary to link these quantities to physical (preferably measurable) flow variables in order to relate the solution to conditions that can be controlled by the experimentalist. Conservation laws that relate the convected quantities, physical variables and transverse particle displacement are summarized in section 3. Section 4 discusses the implications of imposing causality on the solution and shows that the transverse particle displacement defined in section 3 vanishes at upstream infinity when this condition is imposed. Section 5 shows that the result for the transverse particle displacement can be inserted into these conservation laws to obtain an appropriate set of upstream boundary conditions that link the arbitrary convected quantities to the physical flow variables. Section 6 shows how the Fourier transforms of these boundary conditions can be used to relate the spectra of the convected quantities to the spectra of the physical variables that would actually be measured in an experiment. The results are then used to obtain a formula for the sound radiation produced by the interaction of a two-dimensional jet with the trailing edge of a flat plate that extends the result derived in GAL. The formula is used to obtain numerical predictions that are compared with data taken at NASA Glenn Research Center (Zaman, Brown & Bridges, 2013; Bridges, Brown & Bozak, 2014 ; Brown, 2015) as part of a large experimental campaign to study jet-surface interaction noise (Brown, 2012 ; Bridges, 2014). The comparisons were carried out over a broader range of parameters than those in GAL and the agreement is now significantly improved relative to those results. The solution is also used to discuss the effects of imposing causality.

2. Review of basic formalism and comparison with the Orr result

As in G78 , G79 and GAL the flow is assumed to be inviscid and non-heat conducting and the fluid is assumed to be an ideal gas so that the entropy is proportional to $\ln\left(p/\rho^{\gamma}\right)$ and the squared sound speed is equal to $\gamma p/\rho$, where p denotes the pressure, ρ the density and γ the specific heat ratio. Then the pressure $p' = p - p_0$ and mass flux

$$\mathrm{u_i} \equiv \rho v_{\mathrm{i}}', \tag{2.1}$$

perturbations (where v_i' denotes the velocity perturbation) on a transversely sheared mean flow with pressure p_0 =constant, velocity $U\left(\boldsymbol{y}_T\right)$ and mean sound speed squared $c^2\left(\boldsymbol{y}_T\right)$, are governed by the linearized Euler equations

$$\frac{D_0 u_i}{D\tau} + \delta_{1i} u_j \frac{\partial U}{\partial y_j} + \frac{\partial}{\partial y_i} p' = 0 \tag{2.2}$$

and

$$\frac{D_0 p'}{D\tau} + \frac{\partial}{\partial y_j} c^2 u_j = 0, \tag{2.3}$$

where $\boldsymbol{y}_T = \{y_2, y_3\}$, $\boldsymbol{y} = \{y_1, y_2, y_3\} = \{y_1, \boldsymbol{y}_T\}$ and $D_o / D\tau \equiv \partial / \partial\tau + U\partial / \partial y_1$ denotes the convective derivative.

G79 shows that the solution to these equations can be expressed in terms of the two arbitrary convected functions $\tilde{\omega}_c\left(\tau - \frac{y_1}{U}, \boldsymbol{y}_T\right)$ and $\vartheta\left(\tau - (y_1/U), \boldsymbol{y}_T\right)$ and a potential function ϕ that satisfies

$$L_a \phi = -\tilde{\omega}_c\left(\tau - \frac{y_1}{U}, \boldsymbol{y}_T\right), \tag{2.4}$$

where

$$L_a \equiv \frac{D_0^3}{D\tau^3} - \frac{\partial}{\partial y_i} c^2 \left(\frac{\partial}{\partial y_i} \frac{D_0}{D\tau} + 2 \frac{\partial U}{\partial y_i} \frac{\partial}{\partial y_1} \right). \tag{2.5}$$

and the physical variables p' and u_i are determined by

$$p' = -\frac{D_0^3 \phi}{D\tau^3}, \tag{2.6}$$

and

$$u_i = \left(\delta_{ij} \frac{D_0}{D\tau} - \delta_{i1} \frac{\partial U}{\partial y_j} \right) \lambda_j + \varepsilon_{ijk} \frac{1}{c^2} \frac{\partial U}{\partial y_j} \frac{\partial}{\partial y_k} \vartheta\left(\tau - \frac{y_1}{U}, \boldsymbol{y}_T \right), \tag{2.7}$$

with δ_{ij} denoting the Kronecker delta, ε_{ijk} the alternating tensor and

$$\lambda_j \equiv \frac{\partial}{\partial y_j} \frac{D_0 \phi}{D\tau} + 2 \frac{\partial U}{\partial y_j} \frac{\partial \phi}{\partial y_1} \tag{2.8}$$

denoting a kind of generalized particle displacement.

It is well known that the mass flux perturbation, u_i can be eliminated between (2.2) and (2.3) to show that the pressure fluctuation p' satisfies Rayleigh's equation

$$L\, p' = 0, \tag{2.9}$$

where

$$L \equiv \frac{D_o}{D\tau} \left(\frac{\partial}{\partial y_i} c^2 \frac{\partial}{\partial y_i} - \frac{D_o^2}{D\tau^2} \right) - 2 \frac{\partial U}{\partial y_j} \frac{\partial}{\partial y_1} c^2 \frac{\partial}{\partial y_j} \tag{2.10}$$

denotes the usual Rayleigh operator, which is easily shown to be adjoint to the operator L_a

For reasons given in the introduction our focus here is on the steady state (i.e. time stationary) solutions (which are assumed to exist) and we suppose that ϕ is a stationary random variable (Weiner,1938) and therefore that initial conditions imposed in the distant past have all decayed out at the finite time t. A formal steady state solution to (2.4) can then be written as

$$\phi(\mathbf{x},t) = -\int_{-T}^{T}\int_{V} g(\mathbf{y},\tau\,|\,\mathbf{x},t)\,\tilde{\omega}_c\left(\tau - \frac{y_1}{U(\mathbf{y}_T)}, \mathbf{y}_T\right) d\mathbf{y}d\tau$$

$$+\int_{-T}^{T}\int_{S} \hat{n}_j c^2\left[g(\mathbf{y},\tau\,|\,\mathbf{x},t)\lambda_j - \frac{\partial g(\mathbf{y},\tau\,|\,\mathbf{x},t)}{\partial y_j}\frac{D_0\phi}{D\tau}\right] dS(\mathbf{y})\,d\tau \qquad (2.11)$$

where $g(\mathbf{y},\tau\,|\,\mathbf{x},t)$ denotes the Rayleigh operator Greens function which exhibits incoming wave behaviour as $|\mathbf{y}| \to \infty$ and satisfies

$$L\, g(\mathbf{y},\tau\,|\,\mathbf{x},t) = \delta(\mathbf{y}-\mathbf{x})\delta(\tau - t), \qquad (2.12)$$

the first two arguments of $g(\mathbf{y},\tau\,|\,\mathbf{x},t)$ denote the dependent variables and the second two denote the source variables, T denotes a very large but finite time interval, V is a region of space bounded by cylindrical (i.e., parallel to the mean flow) surface(s) S that can be finite, semi-infinite or infinite in the streamwise direction and $\hat{\mathbf{n}} = \{\hat{n}_i\}$ is the unit outward-drawn normal to S. The upper limit $+T$ of the $\tau-$integration can be replaced by t since $g(\mathbf{y},\tau\,|\,\mathbf{x},t) = 0$ for $\tau > t$. The lower limit $-T$ reflects the fact that the initial conditions must be imposed in the distant past in order to insure that they don't contribute to the steady state solution.

Equation (2.11)expresses the solution to equation(2.4) in terms of the volume source distribution $\tilde{\omega}_c(\tau - y_1/U(\mathbf{y}_T), \mathbf{y}_T)$ and the values of the potential ϕ on some arbitrary cylindrical surfaces S (some or all of which may be at infinity). The analysis is somewhat unconventional in that the direct Green's function g now plays the role of an adjoint Green's function for the solution ϕ.

The surface integrals in (2.11) drop out when any of the surfaces S are at infinity (i.e. when V represents all of space) and they can be eliminated when they are not by requiring that the Green's function g satisfy certain boundary conditions on the bounding these surfaces (since g is not uniquely determined by (2.12)). Equation (2.11) then becomes

$$\phi(\mathbf{x},t) = -\int_{-T}^{T}\int_{V} g(\mathbf{y},\tau\,|\,\mathbf{x},t)\,\tilde{\omega}_c\left(\tau - \frac{y_1}{U(\mathbf{y}_T)}, \mathbf{y}_T\right) d\mathbf{y}d\tau \qquad (2.13)$$

Equations (2.6) and (2.13) show that the pressure perturbation p' is then given by

$$p'(\mathbf{x},t) = \int_{-T}^{T}\int_{V} \frac{D_0^3 g(\mathbf{y},\tau\,|\,\mathbf{x},t)}{Dt^3}\,\tilde{\omega}_c\left(\tau - \frac{y_1}{U(\mathbf{y}_T)}, \mathbf{y}_T\right) d\mathbf{y}d\tau \qquad (2.14)$$

while equations (2.7)and (2.8)show that the corresponding transverse velocity perturbation,

$$u_\perp(\mathbf{x},t) \equiv u_i(\mathbf{x},t)\frac{\partial U}{\partial x_i}/|\nabla U| \qquad (2.15)$$

is given by

$$u_{\perp} = -\frac{\partial U / \partial x_i}{|\nabla U|} \int_{-T}^{T} \int_{V} g_i(\boldsymbol{y}, \tau \mid \boldsymbol{x}, t) \tilde{\omega}_c\left(\tau - \frac{y_1}{U(\boldsymbol{y}_T)}, \boldsymbol{y}_T\right) d\boldsymbol{y} d\tau, \tag{2.16}$$

where

$$g_i(\boldsymbol{y}, \tau \mid \boldsymbol{x}, t) \equiv \frac{D_0}{Dt}\left(\frac{\partial}{\partial x_i}\frac{D_0}{Dt} + 2\frac{\partial U}{\partial x_i}\frac{\partial}{\partial x_1}\right) g(\boldsymbol{y}, \tau \mid \boldsymbol{x}, t). \tag{2.17}$$

Inserting equation (B.12) of Goldstein et al 2013b into this result, noting that the integral over the second term vanishes and that the relevant Poisson's-equation Green's function is self-adjoint (i.e., $g_0(\boldsymbol{y}, \tau \mid \boldsymbol{x}, t) = g_0(\boldsymbol{x}, t \mid \boldsymbol{y}, \tau)$) shows that it reduces to (1.4) for two dimensional incompressible flows with constant mean shear when the arbitrary convected quantity $\tilde{\omega}_c\left(\tau - y_1 / U(\boldsymbol{y}_T), \boldsymbol{y}_T\right)$ is replaced by the renormalized convected quantity

$$\omega_c\left(\tau - y_1 / U(\boldsymbol{y}_T)\boldsymbol{y}_T\right) \equiv \tilde{\omega}_c\left(\tau - y_1 / U(\boldsymbol{y}_T), \boldsymbol{y}_T\right)|\nabla U| / \rho c^2, \tag{2.18}$$

which has dimensions of vorticity (based on the rescaled velocity u_i). Equation(2.16) which, like(2.14), does not depend on the second arbitrary convected quantity $\vartheta\left(\tau - y_1 / U, \boldsymbol{y}_T\right)$) is, therefore, a generalization of the Orr result(1.4). The most significant difference is that the convected quantity ω_c is no longer equal to the spanwise vorticity.

GAL show that (2.14) will even apply even when solid surfaces and accompanying downstream wakes are present in the flow if $g(\boldsymbol{y}, \tau \mid \boldsymbol{x}, t)$ and $\vartheta\left(\tau - y_1 / U, \boldsymbol{y}_T\right)$ are required to satisfy appropriate boundary conditions on these surfaces and $g(\boldsymbol{y}, \tau \mid \boldsymbol{x}, t)$ is required to satisfy appropriate jump conditions across the downstream wakes. The formulas (2.14) and (2.16)for the physical variables p' and $u_{\perp}$ can then be viewed as formal solutions to the complete non-homogeneous RDT problem (in the usual case where the solid surfaces are aligned with the constant velocity surfaces). They effectively reduce the RDT problem to the problem of finding the Rayleigh's equation Green's function that satisfies the appropriate boundary conditions on the bounding surfaces S . The solution $p'(\boldsymbol{x}, t)$ will then be independent of the second convected quantity $\vartheta\left(\tau - y_1 / U, \boldsymbol{y}_T\right)$ and the acoustic field will only depend on the single convected quantity $\tilde{\omega}_c\left(\tau - y_1 / U(\boldsymbol{y}_T), \boldsymbol{y}_T\right)$.

In the absence of scattering surfaces and other external sources the unsteady flow (2.14)- (2.17)consists entirely of subsonically propagating disturbances when the mean flow is purely subsonic and, therefore, cannot radiate to the far field (Goldstein, 2005 & 2009). This can easily be verified in any particular case by working out the relevant far field expansion. It is therefore appropriate to identify it with the hydrodynamic component of the motion.

3. Conservation laws for $\tilde{\omega}_c$, ϑ, transverse particle displacement and physical variables

This section summarizes the conservation laws derived in in Goldstein et al (2013b) and G79 that relate the arbitrary convected quantities $\tilde{\omega}_c\left(\tau - y_1/U, \boldsymbol{y}_T\right)$ and $\vartheta\left(\tau - y_1/U, \boldsymbol{y}_T\right)$ and a quantity, which we refer to as the transverse particle displacement, to the physical variables. The next section shows that this transverse particle displacement vanishes when $y_1 \to -\infty$ and section 5 shows how these results can be used to obtain upstream boundary conditions that relate $\tilde{\omega}_c\left(\tau - y_1/U, \boldsymbol{y}_T\right)$ and $\vartheta\left(\tau - y_1/U, \boldsymbol{y}_T\right)$ to the physical (hopefully measurable) flow variables.

The conservation laws, which are given by equations (3.1) and (3.2) of Goldstein et al (2013b), can be written as

$$\frac{\partial}{\partial y_1}\left(\tilde{\omega}_c - p' - \frac{\partial N_i}{\partial y_i}\eta_\perp\right) = N_k \Gamma_{k,0} + \left(\frac{\partial N_k}{\partial y_i} - \frac{\partial N_i}{\partial y_k}\right)\Gamma_{k,i} \qquad \mathbf{(3.1)}$$

$$N_i\left(\varepsilon_{ijk}\Gamma_{k,j} + \varepsilon_{ij1}\frac{\partial \eta_\perp}{\partial y_j}\right) = 0 \qquad (3.2)$$

where $\tilde{\omega}_c$ is related to the rescaled vortical-like quantity ω_c by(2.18) ,

$$N_i \equiv \frac{c^2}{\left|\nabla U\right|^2}\frac{\partial U}{\partial y_i}, \qquad (3.3)$$

$$\Gamma_{k,0}\left(\boldsymbol{y},\tau\right) \equiv \nabla^2\left(u_k - u_k^{(c)}\right) - \frac{\partial}{\partial y_k}\nabla\bullet\left(\boldsymbol{u} - \boldsymbol{u}^{(c)}\right) = \nabla^2\left(u_k - u_k^{(c)}\right) + \frac{\partial}{\partial y_k}\left(c^{-2}\frac{D_0 p'}{D\tau}\right) - \frac{\partial}{\partial y_k}\left[\left(\boldsymbol{u} - \boldsymbol{u}^{(c)}\right)\bullet c^2 \nabla\left(\frac{1}{c^2}\right)\right] \qquad (3.4)$$

and

$$\Gamma_{k,i} \equiv \frac{\partial}{\partial y_i}\left(u_k - u_k^{(c)}\right), \quad \text{for } i = 1,2,3 \qquad (3.5)$$

are source functions and we have used (2.3)to obtain the last member of (3.4).

$$u_k^{(c)} \equiv \varepsilon_{knm}\frac{1}{c^2}\frac{\partial U}{\partial y_n}\frac{\partial \vartheta}{\partial y_m} \qquad (3.6)$$

is the velocity component generated by the second convected quantity ϑ, and

$$\eta_\perp\left(\boldsymbol{x},t\right) \equiv \left(\partial U/\partial x_i\right)\lambda_i = \frac{\partial U}{\partial y_j}\left(\frac{\partial}{\partial y_j}\frac{D_0\phi}{D\tau} + 2\frac{\partial U}{\partial y_j}\frac{\partial \phi}{\partial y_1}\right), \qquad (3.7)$$

is the transverse particle displacement

Equation (2.7) shows that $\eta_\perp$ is related to $u_\perp$ by

$$u_\perp = \frac{1}{\left|\nabla U\right|}\frac{D_0}{D\tau}\eta_\perp \qquad (3.8)$$

which justifies referring to it as the transverse particle displacement.

Equations (3.1) and (3.4)- (3.6) relate the arbitrary convected quantities $\tilde{\omega}_c\left(\tau - y_1 / U\left(\boldsymbol{y}_T\right), \boldsymbol{y}_T\right)$ and $\vartheta\left(\tau - y_1 / U\left(\boldsymbol{y}_T\right), \boldsymbol{y}_T\right)$ to the pressure p', density weighted velocity $\boldsymbol{u}$ and the transverse particle displacement $\eta_\perp$,while equations (3.2) and (3.4)- (3.6) relate the arbitrary convected quantity $\vartheta\left(\tau - y_1 / U\left(\boldsymbol{y}_T\right), \boldsymbol{y}_T\right)$ to the pressure p' , density weighted velocity $\boldsymbol{u}$ and the transverse particle displacement $\eta_\perp$.

The tensor $\left(\partial N_k / \partial y_i - \partial N_i / \partial y_k\right)$is equal to zero and $u_k^{(c)}$ drops out of the first term on the right side of (3.4)for planar base flows, where c^2 and U depend on a single Cartesian coordinate (say y_2) and equation (3.1) then becomes

$$\frac{\partial}{\partial y_1}\left(\tilde{\omega}_c - p' - \frac{dN_2}{dy_2}\eta_\perp\right) = N_2\left[\nabla\cdot\left[c^{-2}\nabla\left(c^2 u_2\right)\right] + \frac{\partial}{\partial y_2}\left(c^{-2}\frac{D_0 p'}{D\tau}\right)\right] \qquad (3.9)$$

which is independent of $u_i^{(c)}$ and, therefore of the second convected quantity ϑ. But the divergence $\partial N_i / \partial y_i$ is equal to zero for the constant shear-constant c^2 parallel mean flow(1.1), since N_i is a constant in that case and it follows from (2.18) that equation (3.9) then reduces to Möhring's (1976) result

$$\frac{\partial}{\partial y_1}\left(\rho\omega_c - \frac{\gamma p'}{c^2}\right) = \nabla\cdot\left[c^{-2}\nabla\left(c^2 u_2\right)\right] + \frac{\partial}{\partial y_2}\left(c^{-2}\frac{D_0 p'}{D\tau}\right) \qquad (3.10)$$

and to Orr's equation (1.3) when the flow is incompressible and two dimensional.

The particle displacement $\eta_\perp$ which appears in equations (3.1) and (3.2) is not actually a physical variable in the usual sense and requires further clarification, which is provided in the next section. However our interest here is in obtaining a set of upstream boundary conditions that relate $\omega_i^{(c)}$ and ϑ to the physically measurable variables at upstream infinity, which can be obtained by taking the limit as $y_1 \to -\infty$ of these equations. This greatly simplifies the formulas and, as will be shown below, even allows us to obtain an explicit formula for $\omega_i^{(c)}$.

4. Particle displacement and causality

As indicated in the paragraphs above and below equations (2.11) and (2.12)our interest is in time stationary solutions which are assumed to exist for the physical variables p' and $u_\perp$. It is therefore appropriate to work with the temporal Fourier transforms

$$\overline{p}'(\boldsymbol{x}:\omega) \equiv \lim_{T\to\infty}\frac{1}{2\pi}\int_{-T}^{T} e^{i\omega t} p'(\boldsymbol{x},t)dt, \quad \overline{u}_\perp(\boldsymbol{x}:\omega) \equiv \lim_{T\to\infty}\frac{1}{2\pi}\int_{-T}^{T} e^{i\omega t} u_\perp(\boldsymbol{x},t)dt\ , \qquad (4.1)$$

where the limits are only formal and the integrals are to be interpreted in a stochastic sense (Weiner, 1938). (Laplace transforms would not be appropriate here.) However the formula (2.13) for the potential ϕ is still only formal in that the integrand on the right hand side has a non-integrable singularity at $\boldsymbol{y}=\boldsymbol{x}$. But the corresponding integrands in equations(2.14) and(2.16) for the physical variables p' and $u_\perp$ remain finite and these quantities are therefore (stochastically) well defined. In fact, GAL, G78 and G79 show that they are given by

$$\bar{p}'(\boldsymbol{x}:\omega)=(2\pi)^2\int_{A_T} e^{i\omega x_1/U(\boldsymbol{y}_T)}\bar{G}_0\left(\boldsymbol{y}_T\,|\,\boldsymbol{x}_T:\omega,\omega/U(\boldsymbol{y}_T)\right)\bar{\Omega}_c(\boldsymbol{y}_T:\omega)\,d\boldsymbol{y}_T, \tag{4.2}$$

and

$$\bar{u}_\perp(\boldsymbol{x}:\omega)=-(2\pi)^2\frac{\partial U}{\partial x_i}\frac{1}{|\nabla U|}\int_{A_T} e^{i\omega x_1/U(\boldsymbol{y}_T)}\bar{G}_i\left(\boldsymbol{y}_T\,|\,\boldsymbol{x}_T:\omega,\omega/U(\boldsymbol{y}_T)\right)\bar{\Omega}_c(\boldsymbol{y}_T:\omega)\,d\boldsymbol{y}_T, \tag{4.3}$$

respectively, where $\boldsymbol{y}_T$ is defined below(2.3), A_T denotes the cross sectional area such that $\int_{A_T}\int_{-\infty}^{\infty}\bullet\, d\boldsymbol{y}_T dy_1=\int_V \bullet\, d\boldsymbol{y}$,$\bar{\Omega}_c(\boldsymbol{x}:\omega)$ is defined as the limit $T\to\infty$ of

$$\bar{\Omega}_c(\boldsymbol{y}_T:\omega,T)\equiv\frac{1}{2\pi}\int_{-T}^{T} e^{i\omega z}\tilde{\omega}_c(z,\boldsymbol{y}_T)\,dz, \tag{4.4}$$

$$\bar{G}_0\left(\boldsymbol{y}_T\,|\,\boldsymbol{x}_T:\omega,\omega/U(\boldsymbol{y}_T)\right)\equiv\lim_{k_1\to\omega/U(\boldsymbol{y}_T)}\bar{G}_0\left(\boldsymbol{y}_\perp\,|\,\boldsymbol{x}_\perp:\omega,k_1\right) \tag{4.5}$$

where

$$\bar{G}_0\left(\boldsymbol{y}_\perp\,|\,\boldsymbol{x}_\perp:\omega,k_1\right)\equiv\frac{\left[ik_1U(\boldsymbol{x}_T)-i\omega\right]^3}{(2\pi)^2}\int_{-\infty}^{\infty}\int_{-\infty}^{\infty} e^{i\left[k_1(y_1-x_1)+\omega(t-\tau)\right]}g(\boldsymbol{y},\tau|\boldsymbol{x},t)d(y_1-x_1)d(t-\tau) \tag{4.6}$$

satisfies the reduced inhomogeneous Rayleigh's equation

$$L_R\bar{G}_0\equiv\frac{1}{(2\pi)^2}\delta(\boldsymbol{x}_T-\boldsymbol{y}_T), \tag{4.7}$$

with L_R being the reduced Rayleigh operator

$$L_R\equiv\nabla_T\bullet\left\{\frac{c^2\nabla_T}{\left[\omega-U(\boldsymbol{y}_T)k_1\right]^2}\right\}+1-\frac{c^2k_1^2}{\left[\omega-U(\boldsymbol{y}_T)k_1\right]^2} \tag{4.8}$$

written in terms of the Laplacian ∇_T with respect to the transverse coordinate $\boldsymbol{y}_T$. Appendix A shows that $\bar{G}_0\left(\boldsymbol{y}_T\,|\,\boldsymbol{x}_T:\omega,\omega/U(\boldsymbol{y}_T)\right)$ remains finite and is continuous at $\boldsymbol{y}_T=\boldsymbol{x}_T$ for two dimensional mean flows and a similar analysis would show that this is true in general, but the notation becomes very tedious in that case. Appendix A also shows that

$$\bar{G}_i\left(\boldsymbol{y}_T \mid \boldsymbol{x}_T : \omega, k_1\right) \equiv \frac{1}{\left[ik_1 U\left(\boldsymbol{x}_T\right) - i\omega\right]} \frac{\partial}{\partial x_i} \bar{G}_0\left(\boldsymbol{y}_T \mid \boldsymbol{x}_T : \omega, k_1\right),\ i = 1,2,3 \tag{4.9}$$

remains finite and continuous at $\boldsymbol{y}_T = \boldsymbol{x}_T$ for two dimensional mean flows. It therefore follows from (4.3), the first line of (B.4), (B.6) and inversion of the Fourier transform (4.1) that

$$\bar{u}_\perp\left(\boldsymbol{x} : \omega\right) \to \frac{e^{i\omega x_1/U(x_2)}}{x_1^2} \bar{\mathcal{U}}_\perp\left(\boldsymbol{x}_T, \omega\right),\ \text{ as } x_1 \to -\infty \tag{4.10}$$

and

$$u_\perp\left(\boldsymbol{x}, t\right) \to \frac{1}{x_1^2} \mathcal{U}_\perp\left(t - x_1 / U\left(x_2\right), \boldsymbol{x}_T\right),\ \text{as } x_1 \to -\infty \tag{4.11}$$

where the purely convected quantity $\mathcal{U}_\perp\left(t - x_1 / U\left(x_2\right), \boldsymbol{x}_T\right)$ is a function of the indicated arguments and $\bar{\mathcal{U}}_\perp\left(\boldsymbol{x}_T, \omega\right)$ is the Fourier transform of that quantity. The comment below (4.8) suggests that these results, which generalize the behavior discussed in the introduction, are expected to apply to much more general transversely sheared mean flows (such as those described below) even though they were derived for two dimensional base flows.

The Fourier transform

$$\bar{\eta}_\perp\left(\boldsymbol{x}, \omega\right) \equiv \lim_{T \to \infty} \frac{1}{2\pi} \int_{-T}^{T} e^{i\omega t} \eta_\perp\left(\boldsymbol{x}, t\right) dt \tag{4.12}$$

of the transverse particle displacement (3.7), which formally satisfies

$$\frac{\partial \bar{\eta}_\perp\left(\boldsymbol{x}, \omega\right)}{\partial x_1} = -\left(2\pi\right)^2 \frac{\partial U}{\partial x_i} \int_{A_T} e^{i\omega x_1/U\left(\boldsymbol{y}_T\right)} \frac{\bar{G}_i\left(\boldsymbol{y}_T \mid \boldsymbol{x}_T : \omega, \omega / U\left(\boldsymbol{y}_T\right)\right)}{U\left(\boldsymbol{x}_T\right) - U\left(\boldsymbol{y}_T\right)} \bar{\Omega}_c\left(\boldsymbol{y}_T : \omega\right) d\boldsymbol{y}_T, \tag{4.13}$$

will become unbounded at $\boldsymbol{y} = \boldsymbol{x}$ since, as shown in Appendix A for the two dimensional case, $\bar{G}_i\left(\boldsymbol{y}_T \mid \boldsymbol{x} : \omega, \omega / U\left(\boldsymbol{y}_T\right)\right)$ will usually not vanish when $\boldsymbol{y}_T = \boldsymbol{x}_T$. It can be made finite in a number of ways. But there is only one possibility if causality is also imposed. This amounts to assuming that the time stationary solutions will exist even if $\eta_\perp\left(\boldsymbol{x}, t\right)$ is assumed to be identically zero in the distant past. This can be accomplished by using the Briggs (1964)-Bers (1975) procedure which amounts to letting ω have a small positive imaginary part, say ε and taking the limit as $\varepsilon \to 0$ of the resulting formula. It is not possible to do this directly in the present case, but (4.13) can represented as the limit of a sequence and this procedure can be used to impose causality on each term of that sequence. It could, however, be argued that $\eta_\perp$ need not be causal because it is not actually a physical variable, but the conservation laws (3.1) -(3.2)and, more importantly, the upstream boundary conditions would then also be non-causal. Our primary interest is in the upstream behaviour of $\eta_\perp$, which will be used to derive the upstream boundary conditions referred to in the introduction. The analysis in Appendix C shows that

$$\frac{\partial \bar{\eta}_\perp(\boldsymbol{x},\omega)}{\partial x_1} \to 0, \text{ as } \quad x_1 \to -\infty \tag{4.14}$$

when causality is imposed, which implies that

$$\frac{\partial \eta_\perp(\boldsymbol{x},t)}{\partial x_1} \to 0, \text{ as } \quad x_1 \to -\infty \tag{4.15}$$

in this case. Different results would be possible if causality were not imposed.

5. Upstream boundary conditions and relation of $\tilde{\omega}_c$, ϑ to the physical variables

It is useful, although not essential, to first split the dependent variables into a hydrodynamic component, which does not directly produce any sound at subsonic Mach numbers, and a non-hydrodynamic component, which accounts for the remaining—including the acoustic—components of the motion, before attempting to derive the relevant boundary conditions. We can then think of the former component as being an upstream 'input' that generates a downstream 'response' when it interacts with streamwise changes in the boundary conditions.

As is well known, it is impossible to unambiguously decompose the unsteady motion on a transversely sheared mean flow into acoustic and hydrodynamic components. We can however require that the hydrodynamic component not radiate any sound at subsonic Mach numbers, with all the acoustic radiation being accounted for by the remaining non-hydrodynamic component. Then, in order to identify the input disturbance with the hydrodynamic component of the motion we divide the Rayleigh equation Green's function $g(\boldsymbol{y},\tau\,|\,\boldsymbol{x},t)$ that appears in the time dependent solution (2.13)-(2.16) into two components, say

$$g(\boldsymbol{y},\tau\,|\,\boldsymbol{x},t) = g^{(H)}(\boldsymbol{y},\tau\,|\,\boldsymbol{x},t) + g^{(s)}(\boldsymbol{y},\tau\,|\,\boldsymbol{x},t), \tag{5.1}$$

where $g^{(H)}(\boldsymbol{y},\tau\,|\,\boldsymbol{x},t)$ denotes a particular solution of (2.12) which is defined on all space when the bounding surfaces S are all at infinity or, more generally, satisfies appropriate boundary conditions (given in Goldstein et al, 2013) on a constant mean velocity surface that extends from minus to plus infinity in the streamwise direction. The corresponding solution, which is given by(2.14) and (2.16) with $g(\boldsymbol{y},\tau\,|\,\boldsymbol{x},t)$ replaced by $g^{(H)}(\boldsymbol{y},\tau\,|\,\boldsymbol{x},t)$, does not produce any acoustic radiation and can, therefore, be identified with the hydrodynamic component of the unsteady motion. The corresponding 'scattered solution' $g^{(s)}(\boldsymbol{y},\tau\,|\,\boldsymbol{x},t)$, satisfies the homogeneous Rayleigh's equation along with appropriate inhomogeneous boundary and jump conditions on the streamwise discontinuous surfaces S and, therefore, accounts for all of the acoustic components of the motion.

We now obtain the relevant upstream boundary conditions for the convected quantities $\tilde{\omega}_c$ and ϑ by taking the upstream limit of (3.1) and (3.2), but with $g(\boldsymbol{y},\tau\,|\,\boldsymbol{x},t)$ replaced by $g^{(H)}(\boldsymbol{y},\tau\,|\,\boldsymbol{x},t)$. This is most easily done by using the frequency representation discussed in section 3. The reduced Rayleigh equation Green's function $\bar{G}(\boldsymbol{y}_T \mid \boldsymbol{x}:\omega,k_1)$ that appears in the frequency domain solutions(4.2),(4.3) and (4.13) then has the decomposition

$$\bar{G}(\boldsymbol{y}_T \mid \boldsymbol{x}:\omega,k_1)=\bar{G}^{(H)}(\boldsymbol{y}_T \mid \boldsymbol{x}:\omega,k_1)+\bar{G}^{(s)}(\boldsymbol{y}_T \mid \boldsymbol{x}:\omega,k_1), \tag{5.2}$$

where $\bar{G}^{(H)}(\boldsymbol{y}_T \mid \boldsymbol{x}:\omega,k_1)$ is either defined on all space when the bounding surfaces S are all at infinity or it satisfies

$$\frac{\hat{n}_j}{\left[\omega-k_1U(\boldsymbol{y}_T)\right]^2}\frac{\partial}{\partial y_j}\bar{G}^{(H)}(\boldsymbol{y}_T \mid \boldsymbol{x}:\omega,k_1)=0, \quad \text{for } \boldsymbol{y}_T\in C_T \tag{5.3}$$

(where C_T denotes the bounding curve/curves that generate the doubly infinite surface/surfaces S) when they are not. The streamwise homogeneous Green's functions $g^{(H)}(\boldsymbol{y},\tau \mid \boldsymbol{x},t)$ and $\bar{G}^{(H)}(\boldsymbol{y}_T \mid \boldsymbol{x}:\omega,k_1)$ will then depend on y_1 and x_1 only in the combination x_1-y_1 and we, therefore, write

$$\bar{G}^{(H)}(\boldsymbol{y}_T \mid \boldsymbol{x}:\omega,k_1)=\bar{G}^{(H)}(\boldsymbol{y}_T \mid \boldsymbol{x}_T:\omega,k_1). \tag{5.4}$$

The convected quantity $\tilde{\omega}_c$ is determined by equations(3.1) and (3.2)whose Fourier transforms are given by

$$\frac{\partial}{\partial y_1}\left[e^{i\omega y_1/U(y_T)}\bar{\Omega}_c(\boldsymbol{y}_T:\omega)-\bar{p}'(\boldsymbol{y}:\omega)\right]-\frac{dN_i}{dy_i}\frac{\partial\bar{\eta}_{\perp}^{(H)}(\boldsymbol{y}_T:\omega)}{\partial y_1}=$$

$$e^{i\omega y_1/U(y_T)}\left[N_k\bar{\Gamma}_{k,0}(\boldsymbol{y}:\omega)+\left(\frac{\partial N_k}{\partial y_i}-\frac{\partial N_i}{\partial y_k}\right)\bar{\Gamma}_{k,i}(\boldsymbol{y}:\omega)\right] \tag{5.5}$$

and

$$N_i\left(\varepsilon_{ijk}\bar{\Gamma}_{k,j}+\varepsilon_{ij1}\frac{\partial\bar{\eta}_{\perp}^{(H)}}{\partial y_j}\right)=0 \tag{5.6}$$

where $\bar{\eta}_{\perp}^{(H)}(\boldsymbol{y}_T:\omega)$ is given by (4.13) with $\bar{G}_i(\boldsymbol{y}_T \mid \boldsymbol{x}:\omega,k_1)$ replaced by $\bar{G}_i^{(H)}(\boldsymbol{y}_T \mid \boldsymbol{x}:\omega,k_1)$

$$\bar{\Omega}_c(\boldsymbol{y}_T:\omega)\equiv\lim_{T\to\infty}\bar{\Omega}_c(\boldsymbol{y}_T:\omega,T) \tag{5.7}$$

and $\bar{\Gamma}_{k,i}(\boldsymbol{y}:\omega)\equiv\lim_{T\to\infty}\bar{\Gamma}_{k,i}(\boldsymbol{y}:\omega,T)$ for $k=0,1,2,3$ with

$$\bar{\Gamma}_{k,i}(\boldsymbol{y}:\omega,T)\equiv\frac{1}{2\pi}\int_{-T}^{T}e^{i\omega[\tau-y_1/U(y_T)]}\Gamma_{k,i}(\boldsymbol{y},\tau)\,d\tau \tag{5.8}$$

where $\Gamma_{k,i}$, for $i=0,1,2,3$, are defined by (3.4) and(3.5).

Then since we have shown that Fourier transform $\bar{\eta}_{\perp}^{(H)}(\boldsymbol{y}_T:\omega)$ of the transverse particle displacement $\eta_{\perp}^{(H)}$ vanishes as $y_1 \to -\infty$ and an argument similar that use to obtain (B.6) shows that $\bar{p}'(\boldsymbol{y}:\omega)$ should vanish like y_1^{-2} as $y_1 \to -\infty$ equations (5.5) and (5.6) imply that

$$\bar{\Omega}_c(\boldsymbol{y}_T:\omega,T) \to \frac{1}{i\omega}U(\boldsymbol{y}_T)\left[N_k\bar{\Gamma}_{k,0}^{\infty}(\boldsymbol{y}:\omega)+\left(\frac{\partial N_k}{\partial y_i}-\frac{\partial N_i}{\partial y_k}\right)\bar{\Gamma}_{k,i}^{\infty}\right], \text{ as } y_1 \to -\infty \tag{5.9}$$

and

$$N_i\varepsilon_{ijk}\bar{\Gamma}_{k,j}^{\infty} \to 0 \tag{5.10}$$

where

$$\bar{\Gamma}_{k,i}^{\infty}(\boldsymbol{y}:\omega,T) \equiv \lim_{y_1\to-\infty}\bar{\Gamma}_{k,i}(\boldsymbol{y}:\omega,T). \tag{5.11}$$

These results provide the desired relation between the convected quantities $\tilde{\omega}_c(\tau - y_1/U(\boldsymbol{y}_T),\boldsymbol{y}_T), \vartheta(\tau - y_1/U(\boldsymbol{y}_T),\boldsymbol{y}_T)$ and the upstream limit $\bar{\Gamma}_{k,i}^{\infty}(\boldsymbol{y}:\omega)$, for $i=0,1,2,3$ of the physically measurable variables that enter through $\Gamma_{k,i}(\boldsymbol{y},\tau)$ in an arbitrary transversely sheared mean flow.

But the focus in the remainder of the paper will be on the two-dimensional mean flows for which $\partial N_k/\partial y_i - \partial N_i/\partial y_k = 0$ and equation (5.9) becomes

$$\hat{\Omega}_c(y_2:\omega,k_3,T) = \frac{1}{i\omega}U(y_2)N_2\hat{\Gamma}_{\infty} \tag{5.12}$$

where

$$\hat{\Omega}_c(y_2;\omega,k_3,T) \equiv \frac{1}{2\pi}\int_{-T}^{T} e^{-iy_3k_3}\bar{\Omega}_c(\boldsymbol{y}_T:\omega,T)\,dy_3 = \frac{1}{(2\pi)^2}\int_{-T}^{T} e^{-iy_3k_3}\int_{-T}^{T} e^{i\omega\xi}\tilde{\omega}_c(\xi,\boldsymbol{y}_T)\,d\xi\,dy_3 \tag{5.13}$$

is the double Fourier transform of the convected quantity $\tilde{\omega}_c(\xi,\boldsymbol{y}_T)$ and

$$\hat{\Gamma}_{\infty}(y_2;\omega,k_3,T) = \frac{1}{2\pi}\int_{-\infty}^{\infty} e^{-iy_3k_3}\bar{\Gamma}_{2,0}^{\infty}(\boldsymbol{y}_T:\omega,T)\,dy_3 = \frac{1}{(2\pi)^2}\lim_{y_1\to-\infty}\int_{-\infty}^{\infty} e^{-iy_3k_3}\int_{-T}^{T} e^{i\omega[\tau-y_1/U(y_T)]}\Gamma_{2,0}(\boldsymbol{y},\tau)\,d\tau\,dy_3 \tag{5.14}$$

is the upstream limit of the Fourier transform of the physically measureable vorticity derivative $\Gamma_{2,0}$ given by(3.4).

But equations(3.4) and (3.6) imply that

$$\Gamma_{2,0}(\boldsymbol{y},\tau) = \nabla^2 u_2 - \frac{\partial}{\partial y_2}\nabla\bullet\boldsymbol{u} = \nabla\cdot\left[c^{-2}\nabla(c^2u_2)\right] + \frac{\partial}{\partial y_2}\left(c^{-2}\frac{D_0p'}{D\tau}\right) \tag{5.15}$$

for two-dimensional mean flows and, therefore that $\Gamma_{2,0}(\boldsymbol{y},\tau)$ and consequently, $\hat{\Gamma}_{\infty}(y_2;\omega,k_3,T)$ only depend on the physical variables u_2 and p' for two-dimensional mean flows. Equation (5.12) therefore provides the desired upstream boundary condition that relates the Fourier transform of the unknown convected quantity $\tilde{\omega}_c\left(\tau - y_1/U\left(\boldsymbol{y}_T\right), \boldsymbol{y}_T\right)$ to the physically measurable quantity (5.15) in this case.

But we can go even further than this since an argument similar to that given at the end of Appendix B can be used to show that p' should vanish like $1/y_1^2$ as $y_1 \to -\infty$ and $\lim_{y_1\to\infty} \Gamma_{2,0}$ is, therefore, given by $\nabla\cdot\left[c^{-2}\nabla\left(c^2 u_2\right)\right]$. Inserting (4.11)into this result, noting that $u_\perp\left(\boldsymbol{x},t\right) = u_2\left(\boldsymbol{x},t\right)$ in this case shows that

$$\nabla\cdot\left[c^{-2}\nabla\left(c^2 u_2\right)\right] \to \frac{\partial^2 u_2}{\partial y_2^2} \to \left[\frac{\partial U\left(y_2\right)/\partial y_2}{U^2\left(y_2\right)}\right]^2 \frac{\partial^2}{\partial\tau^2}\mathcal{U}_2\left(\tau - y_1/U\left(y_2\right), \boldsymbol{y}_T\right),\ y_1 \to -\infty \tag{5.16}$$

Inserting this into (5.8) and (5.11), and integrating the result by parts shows that

$$\bar{\Gamma}^{\infty}_{2,0}\left(\boldsymbol{y}:\omega, T\right) = \bar{\Gamma}^{\infty}_{2,0}\left(\boldsymbol{y}_T:\omega, T\right) = \frac{1}{2\pi}\int_{-T}^{T} e^{i\omega\left[\tau - y_1/U\left(\boldsymbol{y}_T\right)\right]}\Gamma_\infty\left(\boldsymbol{y},\tau\right)d\tau \tag{5.17}$$

where

$$\Gamma_\infty\left(\boldsymbol{y},\tau\right) \equiv \left[\frac{\partial U\left(y_2\right)/\partial y_2}{U^2\left(y_2\right)}\right]^2 \frac{\partial^2}{\partial\tau^2}\mathrm{U}_\perp\left(\tau - y_1/U\left(\boldsymbol{y}_T\right), \boldsymbol{y}_T\right) = \Gamma_\infty\left(\tau - y_1/U\left(\boldsymbol{y}_T\right), \boldsymbol{y}_T\right) \tag{5.18}$$

6. Relation between the $\tilde{\omega}_c$ spectra and measurable turbulence correlations

But only statistical quantities, such as

$$\hat{\Gamma}_\infty\left(\boldsymbol{y},\tau\right)\hat{\Gamma}_\infty\left(\tilde{\boldsymbol{y}},\tau+\tilde{\tau}\right) \equiv \lim_{T\to\infty}\frac{1}{2T}\int_{-T}^{T}\hat{\Gamma}_\infty\left(\boldsymbol{y},\tau\right)\hat{\Gamma}_\infty\left(\tilde{\boldsymbol{y}},\tau+\tilde{\tau}\right)d\tau \tag{6.1}$$

where $\hat{\Gamma}_\infty$ is defined by(5.15) and(5.14), are of interest for the time stationary turbulent flows that are the main focus of RDT. For simplicity, we only consider mean flows that are uniform in the y_3 -direction and suppose that the turbulence is statistically homogeneous in the spanwise direction. Then the space-time average

$$\left\langle\Gamma_\infty\left(\boldsymbol{y},\tau\right)\Gamma_\infty\left(y_1,\tilde{y}_2,y_3+\eta_3,\tau+\tilde{\tau}\right)\right\rangle$$

$$\equiv \lim_{T\to\infty}\frac{1}{2T}\int_{-T}^{T}\int_{-\infty}^{\infty}\Gamma_\infty\left(\boldsymbol{y}_T,\tau - y_1/U\left(y_2\right)\right)\Gamma_\infty\left(\tilde{y}_2,y_3+\eta_3,\tau-\tilde{y}_1/U\left(\tilde{y}_2\right)+\tilde{\tau}\right)d\tau dy_3$$

$$= \lim_{T\to\infty}\frac{1}{2T}\int_{-T}^{T}\int_{-\infty}^{\infty}\Gamma_\infty\left(\boldsymbol{y}_T,\tau\right)\Gamma_\infty\left(\tilde{y}_2,y_3+\eta_3,\tau+\tilde{\tau}-\left[y_1/U\left(\tilde{y}_2\right)-y_1/U\left(y_2\right)\right]\right)d\tau dy_3 \tag{6.2}$$

will exist and be independent of τ, y_3 and it follows from the convolution theorem that

$$\frac{1}{(2\pi)^2}\int_{-\infty}^{\infty}\int_{-\infty}^{\infty} \exp\left\{i\left[\omega\left(\tilde{\tau}-\left[\tilde{y}_1/U(\tilde{y})-y_1/U(y_2)\right]\right)-k_3\eta_3\right]\right\}$$

$$\times\left\langle\Gamma_\infty(\boldsymbol{y},\tau)\Gamma_\infty(\tilde{y}_1,\tilde{y}_2,y_3+\eta_3,\tau+\tilde{\tau})\right\rangle d\tilde{\tau}d\eta_3=(2\pi)^2\lim_{T\to\infty}\frac{\hat{\Gamma}_\infty(y_2;\omega,k_3,T)\left[\hat{\Gamma}_\infty(\tilde{y}_2;\omega,k_3,T)\right]^*}{2T} \quad (6.3)$$

where $\hat{\Gamma}_\infty(y_2;\omega,k_3,T)$ is given by (5.14) and the asterisk denotes the complex conjugate.

It, therefore, follows from (5.12)and(6.3) that

$$S(y_2,\tilde{y}_2:k_3,\omega)\equiv(2\pi)^3\lim_{T\to\infty}\frac{\hat{\Omega}_c(y_2:\omega,k_3;T)\hat{\Omega}_c^*(\tilde{y}_2:\omega,k_3;T)}{2T}$$

$$=\frac{1}{2\pi}\int_{-\infty}^{\infty}\int_{-\infty}^{\infty}e^{i(\omega\tilde{\tau}-k_3\eta_3)}\left\langle\tilde{\omega}_c(t,\boldsymbol{y}_T)\tilde{\omega}_c(t+\tilde{\tau},\tilde{y}_2,y_3+\eta_3)\right\rangle d\tilde{\tau}d\eta_3=\frac{U(y_2)U(\tilde{y}_2)N_2\tilde{N}_2}{2\pi\omega^2}$$

$$\times\int_{-\infty}^{\infty}\int_{-\infty}^{\infty}e^{\left\{i\left[\omega\left(\tilde{\tau}-\left[\tilde{y}_1/U(\tilde{y}_2)-y_1/U(y_2)\right]\right)-k_3\eta_3\right]\right\}}\left\langle\Gamma_\infty(\boldsymbol{y},t)\Gamma_\infty(\tilde{y}_1,\tilde{y}_2,y_3+\eta_3,t+\tilde{\tau})\right\rangle d\tilde{\tau}d\eta_3 \quad (6.4)$$

where $\hat{\Omega}_c(y_2:\omega,k_3,T)$ is given by (5.13).

6.1 Source Model

Since the problem is linear, it follows from(4.3) and (5.13) that the complete solution to any problem where the surface extends continuously from $-\infty<x_3<\infty$, say for the Fourier transformed transverse velocity fluctuation $\bar{u}_\perp(x_1,x_2;k_3,\omega)$, must be of the form

$$\bar{u}_\perp(x_1,x_2;\omega,k_3)=\int_{l_T}\mathcal{R}(y_2|x_1,x_2;\omega,k_3)\hat{\Omega}(y_2:\omega,k_3)dy_2, \quad (6.5)$$

which means that knowledge of $\hat{\Omega}(y_2:\omega,k_3)$ is all that is actually needed for the two dimensional mean flow solutions being considered here. A similar formula would, of course, also hold for Fourier transformed pressure fluctuation $\hat{p}'\left(x_1,x_2;\hat{k},\omega\right)$.

The spectrum, $S(y_2,\tilde{y}_2:k_3,\omega)$ of the convected quantity $\tilde{\omega}_c$, which is related to the cross correlation $\left\langle\Gamma_\infty(\boldsymbol{y},t)\Gamma_\infty(\tilde{y}_1,\tilde{y}_2,y_3+\eta_3,t+\tilde{\tau})\right\rangle$ of the upstream vorticity fluctuation by(6.4) needs to be specified before formulas for the acoustic spectrum such as the one derived in GAL can actually be used. While (5.18)and(5.16) show that

$$\Gamma_\infty(\boldsymbol{y},\tau)=\lim_{y_1\to-\infty}\nabla\cdot\left[c^{-2}\nabla\left(c^2u_2\right)\right] \tag{6.6}$$

and therefore $\left\langle\Gamma_\infty(\boldsymbol{y},t)\Gamma_\infty(\tilde{y}_1,\tilde{y}_2,y_3+\eta_3,t+\tilde{\tau})\right\rangle$ corresponds to a physically measureable correlation, we are unaware of any measurements of this quantity that have actually been carried out . But the transverse velocity correlation $\left\langle v_2'(t,\boldsymbol{y})v_2'(t+\tilde{\tau},\tilde{\boldsymbol{y}})\right\rangle$, which has been extensively measured, can be well represented by the exponential form $A(y_2,\tilde{y}_2)\rho(y_2)\rho(\tilde{y}_2)\{1+a_1(\tilde{\tau}-$

$$\left[\tilde{y}_1/U(\tilde{y}_2)-y_1/U(y_2)\right])\frac{\partial}{\partial\tilde{\tau}}\Big\}\exp-\sqrt{\left[f(\eta_2/l_2)\right]^2+\left\{\tilde{\tau}-\left[\tilde{y}_1/U(\tilde{y}_2)-y_1/U(y_2)\right]\right\}^2/\tau_0^2+(\eta_3/l_3)^2}$$

where the derivative term accounts for the negative tail of the correlation and the amplitude $A(y_2,\tilde{y}_2)$ is expected to vanish as $y_2,\tilde{y}_2\to 0,\infty$. We therefore initially suppose that

$$\left\langle\mathcal{U}_\perp\left(t-y_1/U(y_2),\boldsymbol{y}_T\right)\mathcal{U}_\perp\left(t+\tilde{\tau}-\tilde{y}_1/U(\tilde{y}_2),\tilde{y}_2,y_3+\eta\right)\right\rangle=$$

$\lim_{y_1\to-\infty}y_1^4\left\langle u_\perp(y_1,\boldsymbol{y}_T,t)u_\perp(y_1,\tilde{\boldsymbol{y}}_T,t+\tilde{\tau})\right\rangle=\lim_{y_1\to-\infty}y_1^4\left\langle\rho v_\perp'(y_1,\boldsymbol{y}_T,t)\rho v_\perp'(y_1,\tilde{\boldsymbol{y}}_T,t+\tilde{\tau})\right\rangle$ can be modelled by

$$\left\langle\mathcal{U}_\perp\left(t-y_1/U(y_2),\boldsymbol{y}_T\right)\mathcal{U}_\perp\left(t+\tilde{\tau}-\tilde{y}_1/U(\tilde{y}_2),\tilde{y}_2,y_3+\eta_3\right)\right\rangle=$$

$$A(y_2,\tilde{y}_2)l_2^4\rho(y_2)\rho(\tilde{y}_2)\left\{1+a_1\left(\tilde{\tau}-\left[\tilde{y}_1/U(\tilde{y}_2)-y_1/U(y_2)\right]\right)\frac{\partial}{\partial\tilde{\tau}}+\ldots\right\}$$

$$\times\exp-\sqrt{\left[f(\eta_2/l_2)\right]^2+\left\{\tilde{\tau}-\left[\tilde{y}_1/U(\tilde{y}_2)-y_1/U(y_2)\right]\right\}^2/\tau_0^2+(\eta_3/l_3)^2} \tag{6.7}$$

which as shown (5.18) is related to $\left\langle\Gamma_\infty(\boldsymbol{y},t)\Gamma_\infty(\tilde{y}_1,\tilde{y}_2,y_3+\eta_3,t+\tilde{\tau})\right\rangle$ by

$$\left\langle\Gamma_\infty(\boldsymbol{y},t)\Gamma_\infty(\tilde{y}_1,\tilde{y}_2,y_3+\eta_3,t+\tilde{\tau})\right\rangle=\left[\frac{(dU/dy_2)(dU/d\tilde{y}_2)}{U^2(\tilde{y}_2)U^2(y_2)}\right]^2\frac{\partial^4}{\partial\tau^4}\left\langle\mathrm{U}_\perp\left(t-y_1/U(y_2),\boldsymbol{y}_T\right)\right.$$

$$\left.\times\mathrm{U}_\perp\left(t+\tilde{\tau}-\tilde{y}_1/U(\tilde{y}_2),\tilde{y}_2,y_3+\eta\right)\right\rangle \tag{6.8}$$

Equation (40) of Leib & Goldstein (2011) can be used to show that the spectrum (6.3) of this quantity is given by the following Hankel transform

$$\int_{-\infty}^{\infty}\int_{-\infty}^{\infty}e^{i\left[\omega\left(\tilde{\tau}-\left[\tilde{y}_1/U(\tilde{y}_2)-y_1/U(y_2)\right]\right)-k_3\eta_3\right]}\left\langle\Gamma_\infty(\boldsymbol{y},t)\Gamma_\infty(\tilde{y}_1,\tilde{y}_2,y_3+\eta_3,t+\tilde{\tau})\right\rangle d\tilde{\tau}d\eta_3=2\pi\tau_0l_3l_2^4$$

$$\times A(y_2,\tilde{y}_2)\rho(y_2)\rho(\tilde{y}_2)\left[\frac{\partial U/\partial y_2}{U^2(y_2)}\frac{\partial U/\partial \tilde{y}_2}{U^2(\tilde{y}_2)}\omega^2\right]^2\left[1-a_1\left(1+\omega\frac{\partial}{\partial\omega}\right)+\ldots\right]$$

$$\times\int_0^\infty J_0\left(r\sqrt{(\omega\tau_0)^2+(k_3l_3)^2}\right)e^{-\sqrt{[f(\eta_2/l_2)]^2+r^2}}rdr \qquad (6.9)$$

And it follows from equations (A.14) and (A.18) of Afsar, Sescu and Leib (2016) that

$$\int_{-\infty}^{\infty}\int_{-\infty}^{\infty}e^{i\left[\omega\left(\tilde{\tau}-\left[\tilde{y}_1/U(\tilde{y}_2)-y_1/U(y_2)\right]\right)-k_3\eta_3\right]}\left\langle\Gamma_\infty(\boldsymbol{y},t)\Gamma_\infty(\tilde{y}_1,\tilde{y}_2,y_3+\eta_3,t+\tilde{\tau})\right\rangle d\tilde{\tau}d\eta_3=-2\pi\tau_0A(y_2,\tilde{y}_2)$$

$$\times l_3l_2^4\rho(y_2)\rho(\tilde{y}_2)\left[\frac{\partial U/\partial y_2}{U^2(y_2)}\frac{\partial U/\partial \tilde{y}_2}{U^2(\tilde{y}_2)}\omega^2\right]^2\left[1-a_1\left(1+\frac{(\omega\tau_0)^2}{\chi}\frac{\partial}{\partial\chi}\right)+\ldots\right]\frac{1}{\chi}\frac{\partial}{\partial\chi}\left(\frac{e^{-|f(\eta_2/l_2)|\chi}}{\chi}\right) \qquad (6.10)$$

where

$$\chi\equiv\sqrt{1+(\omega\tau_0)^2+(k_3l_3)^2} \qquad (6.11)$$

and equation(6.4) then shows that

$$S(y_2,\tilde{y}_2:k_3,\omega)=-\left(\rho_\infty c_\infty^2\right)^2\tau_0l_2^4l_3A(y_2,\tilde{y}_2)\left[\frac{dU}{dy_2}\frac{dU}{d\tilde{y}_2}\frac{\omega^2}{U^3(\tilde{y}_2)U^3(y_2)}\right]$$

$$\times\left[1-a_1\left(1+\frac{(\omega\tau_0)^2}{\chi}\frac{\partial}{\partial\chi}\right)+\ldots\right]\frac{1}{\chi}\frac{\partial}{\partial\chi}\left(\frac{e^{-|f(\eta_2/l_2)|\chi}}{\chi}\right) \qquad (6.12)$$

since ρc^2 is constant in transversely sheared flows.

7. Application to a large aspect ratio rectangular jet

The problem of a two-dimensional jet interacting with the trailing edge of a flat plate is currently of considerable interest because of its relevance to understanding noise production in future aircraft configurations such as that shown in figure 3 in which the engine exhaust is of a very wide aspect ratio on an almost rectangular jet.

Figure 3 Proposed aircraft configuration

GAL analyzed the model problem shown in figure 4 in order to represent the interaction between a jet emanating from a large-aspect ratio rectangular nozzle with the trailing edge of a flat plate and compared the results with recent experiments on this configuration that were performed at NASA Glenn Research Center (Zaman, Brown and Bridges 2013; Brown, 2015).

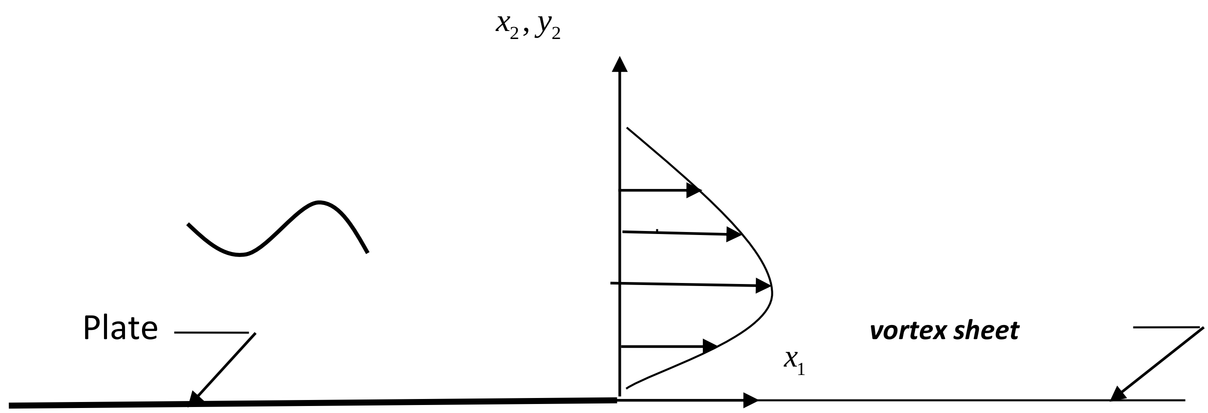

Figure 4 Computational model of the Jet/surface interaction problem

They considered the general case where the mean flow is non-zero at the surface of the plate and therefore leaves the trailing edge with different velocities above and below the interface. But, as shown below, the surface velocity is relatively small compared to the maximum velocity and will therefore be set to zero in the present computation: In which case their analysis, which minimizes the trailing edge singularity (i.e. imposes a Kutta condition) and uses the Wiener- Hopf method to calculate the Green's function, shows that the acoustic spectrum

$$I_\omega(\boldsymbol{x}) \equiv \frac{1}{2\pi}\int_{-\infty}^{\infty} e^{i\omega\tilde{\tau}}\, \widetilde{p^s(\boldsymbol{x},t)\, p^s(\boldsymbol{x},t+\tilde{\tau})}\, d\tilde{\tau} \tag{7.1}$$

where $\tilde{\bullet}$ denotes the time average, is given by

$$I_\omega(\boldsymbol{x}) = \left(\frac{(2\pi)^2 k_\infty \sin\theta \sin\psi}{|\boldsymbol{x}|}\right)^2 \int_0^\infty\int_0^\infty \Phi_{\lessgtr}\left(k_1^{(s)}, k_3^{(s)}, y_2, \omega\right) \Phi^*_{\lessgtr}\left(k_1^{(s)}, k_3^{(s)}, \tilde{y}_2, \omega\right)$$

$$\times \bar{G}\left(y_2 \middle| 0 : k_3^{(s)}, \omega / U(y_2), \omega\right) \bar{G}^*\left(\tilde{y}_2 \middle| 0 : k_3^{(s)}, \omega / U(\tilde{y}_2), \omega\right) S\left(y_2, \tilde{y}_2 : k_3^{(s)}, \omega\right) dy_2 d\tilde{y}_2, \tag{7.2}$$

for $x_2 \lessgtr 0$ where $S\left(y_2, \tilde{y}_2 : k_3^{(s)}, \omega\right)$ is defined by (6.4),

$$k_\infty \equiv \omega / c_\infty \tag{7.3}$$

$$k_1^{(s)} = k_\infty \cos\theta, \;\; k_3^{(s)} = k_\infty \sin\theta \cos\psi \tag{7.4}$$

$$\Phi_{\lessgtr}\left(k_1,k_1,y_2,\omega\right)\equiv\frac{\kappa_-\left(k_1,k_3,\omega\right)A_{\lessgtr}}{\kappa_+\left(\omega/U\left(y_2\right),k_3,\omega\right)\left[\omega/U\left(y_2\right)-k_1\right]\hat{P}'_{\lessgtr}\left(0;k_1,k_3,\omega\right)} \tag{7.5}$$

$$\frac{A_<}{\hat{P}'_<\left(0;k_1,k_3,\omega\right)}=\frac{1}{\sqrt{k_1^2+k_3^2-k_\infty^2}} \tag{7.6}$$

$$\bar{G}\left(y_2\middle|0:k_3^{(s)},\omega/U\left(y_2\right),\omega\right)=\frac{\omega^2P_>\left(y_2:\omega,\omega/U\left(y_2\right),k_3\right)}{\left(2\pi\right)^3c_s^2P'_>\left(0:\omega,\omega/U\left(y_2\right),k_3\right)} \tag{7.7}$$

$\kappa_\pm\left(k_1,k_3,\omega\right)$ denote bounded analytic functions in the upper/lower half planes that satisfy the factorization condition

$$\frac{\kappa_+\left(k_1,k_3,\omega\right)}{\kappa_-\left(k_1,k_3,\omega\right)}=\frac{P_>\left(0:\omega,k_1,k_3\right)}{P'_>\left(0:\omega,k_1,k_3\right)}-\frac{1}{\sqrt{k_1^2+k_3^2-k_\infty^2}} \tag{7.8}$$

$P_{\lessgtr}\left(y_2:\omega,k_1,k_3\right)$ denote homogeneous solutions to (A.3) that have outgoing wave behavior as $y_2\to\mp\infty$, θ denotes the polar angle measured from the downstream x_1 axis and ψ denotes the azimuthal angle measured from the plane of the plate.

GAL considered the low frequency limit $k_3=O\left(k_\infty\right),k_\infty\ll1$ and obtained the result given by equation (6.33) of their paper, which has the advantage of being much more explicit than the exact $O(1)$ result but does not adequately describe the high frequency sound field produced by the trailing edge interaction. It does, however, adequately describe the experimentally observed low-frequency spectrum when the negative tail in transverse velocity correlation is included (Afsar et al 2017).

The high frequency spectrum can be described by using the WKBJ method to obtain the high frequency outgoing wave homogeneous solution

$$P_>\left(y_2:\omega,k_1,k_3\right)=\frac{1-\hat{k}_1M\left(y_2\right)}{\left[q\left(y_2\middle|\hat{k}_1,\hat{k}_3\right)\right]^{1/4}}\exp\left(ik_\infty\int_0^{y_2}\sqrt{q\left(y\middle|\hat{k}_1,\hat{k}_3\right)}dy\right) \tag{7.9}$$

to (A.3)(Goldstein, 1979a) where

$$\hat{k}_n\equiv k_n/k_\infty,\quad n=1,3 \tag{7.10}$$

and

$$q\left(y\middle|\hat{k}_1,\hat{k}_3\right)\equiv\left[1-\hat{k}_1M\left(y\right)\right]^2-\hat{k}_1^2-\hat{k}_3^2 \tag{7.11}$$

and inserting the result into equations (7.4)-(7.7) to obtain the following

$$\frac{\kappa_+(k_1,k_3,\omega)}{\kappa_-(k_1,k_3,\omega)}=\frac{-2}{\sqrt{k_1^2+k_3^2-k_\infty^2}} \tag{7.12}$$

$$\kappa_-(k_1,k_3,\omega)=-\frac{1}{2}\sqrt{k_1-k_\infty\left(1-\sin^2\theta\cos^2\psi\right)^{1/2}} \tag{7.13}$$

$$\kappa_+(k_1,k_3,\omega)=\frac{1}{\sqrt{k_1+k_\infty\left(1-\sin^2\theta\cos^2\psi\right)^{1/2}}} \tag{7.14}$$

It, therefore, follows that follows that

$$\Phi_<\left(k_1^{(s)},k_1^{(s)},y_2,\omega\right)=\frac{-M^{1/2}(y_2)\sqrt{1+\beta M(y_2)}}{2k_\infty\left[1-M(y_2)\cos\theta\right]\sqrt{\beta+\cos\theta}} \tag{7.15}$$

and

$$\bar{G}\left(y_2|0:k_3^{(s)},\omega/U(y_2),\omega\right)=\frac{-ik_\infty\exp\left(ik_\infty\int_0^{y_2}\sqrt{q(y|y_2)}dy\right)}{(2\pi)^3\left[q(0|y_2)q(y_2|y_2)\right]^{1/4}} \tag{7.16}$$

where

$$q(y|y_2)\equiv q\left(y|1/M(y_2),\sin\theta\cos\psi\right) \tag{7.17}$$

and equation (7.2) then becomes

$$I_\omega(\boldsymbol{x})=\left(\frac{k_\infty}{4\pi|\boldsymbol{x}|}\right)^2(\beta-\cos\theta)\int_0^\infty\int_0^\infty \frac{\left[M(y_2)M(\tilde{y}_2)\right]^{3/2}Q(y_2|\theta,\varphi)\left[Q(\tilde{y}_2|\theta,\varphi)\right]^*}{\left[1-M(y_2)\cos\theta\right]\left[1-M(\tilde{y}_2)\cos\theta\right]}$$

$$\times\frac{S\left(y_2,\tilde{y}_2:k_3^{(s)},\omega\right)}{\sqrt{\left[1-\beta M(y_2)\right]\left[1-\beta M(\tilde{y}_2)\right]}}dy_2d\tilde{y}_2, \tag{7.18}$$

for $x_2<0$ where

$$Q(y_2|\theta,\varphi)\equiv\left[\frac{q(0|y_2)-e^{-\chi_0k_\infty}}{q(y_2|y_2)}\right]^{1/4}\exp\left(ik_\infty\int_0^{y_2}\sqrt{q(y|y_2)}dy\right) \tag{7.19}$$

$$\beta\equiv\left(1-\sin^2\theta\cos^2\psi\right)^{1/2}, \tag{7.20}$$

$M(y_2)=U(y_2)/c_\infty$ denotes the local acoustic Mach number at the position y_2, χ_0 is a positive constant and we have inserted the exponential damping factor $e^{-\chi_0k_\infty}$ into (7.19), which leaves the asymptotic expansion unchanged to the order of approximation considered here. In other words, it is asymptotically equivalent to the straight forward result. It reduces to the low frequency result (6.33) of GAL when $Q(y_2|\theta,\varphi)=1$.But $Q(y_2|\theta,\varphi)$ also $\rightarrow 1$ as $k_\infty \rightarrow 0$ and equation(7.18), therefore, behaves like (but is not identical to) a uniformly valid composite solution that applies at all frequencies.

It is, of course necessary to insert a formula for the source function S into (7.18) before using these results to calculate the acoustic field. GAL used a rather complicated approximate procedure to relate this quantity to an experimentally measurable turbulence correlation. The present analysis allows us to use the much simpler and more general exact relation(6.4) and model the turbulence correlation to obtain the explicit formula (6.12) for S .

As indicated above, the model problem considered in this section can be used to represent the interaction between a jet emanating from a large-aspect ratio rectangular nozzle with the trailing edge of a flat plate. The analysis is basically inviscidbut accounts for viscous effects by imposing a Kutta condition at the trailing edge (GAL). Brown and Daniels (1975) use high Reynolds number asymptotic analysis to show that this condition is consistent with the viscous boundary layer flow at the trailing edge. The importance of impsoing a Kutta condition in inviscid analyses involving an edge has been reviewed and discussed by Crighton (1985) and Ayton, Gill and Peake (2016).

Recent experiments on this configuration were performed at NASA Glenn Research Center (Zaman, Brown and Bridges 2013; Brown, 2015). The relevant geometric parameters are shown in figure 5.

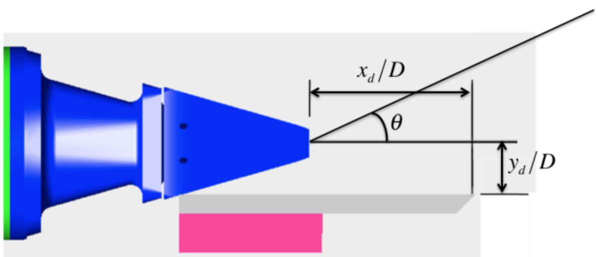

Figure 5 Nozzle/plate configuration. Figure courtesy Dr. James E. Bridges, NASA Glenn.

We assume that the mean density ρ is constant and the mean velocity profile $U(y_2)$ can be represented by the twice differentiable function

$$U(y_2)=U_d\begin{cases}\left[\dfrac{(t_d/2)^2-(y_2-y_d)^2}{(t_d/2)^2}\right]^2 e^{-(y_2-y_d)^2\kappa^2}, & \text{for } (y_2-y_d)^2<(t_d/2)^2 \\ 0, & \text{for } (y_2-y_d)^2>(t_d/2)^2\end{cases} \tag{7.21}$$

with compact support $|y_2-y_d|\le t_d/2$, where y_d is the distance from the plate to the nozzle centerline (see Fig. 5), t_d is the thickness of the jet and κ controls the profile decay.

Since the factor $A(y_2,\tilde{y}_2)$ in (6.7) must vanish at the jet boundaries and is determined by strength of the turbulence at the source location, we expect $A(y_2,y_2)$ to be proportional to the turbulence intensity at y_2 which is roughly proportional to the mean velocity gradient at that point. We therefore set

$$A(y_2,\tilde{y}_2)\equiv A_0\sqrt{\left|dU(y_2)/dy_2\right|\left|dU(\tilde{y}_2)/d\tilde{y}_2\right|}\left[\alpha(y_2)\alpha(\tilde{y}_2)\right]+B_0U(y_2)U(\tilde{y}_2) \qquad (7.22)$$

where B_0 and A_0 are constants and the factor

$$\alpha(y_2)=\begin{cases}\left[(t_d/2)^2-(y_2-y_d)^2\right]^3, & \text{for } (y_2-y_d)^2<(t_d/2)^2\\ 0, & \text{for } (y_2-y_d)^2>(t_d/2)^2\end{cases} \qquad (7.23)$$

is inserted to insure that the turbulence correlation (6.8)vanishes at the jet boundaries.

Measurements of the noise generated by the interaction of rectangular jets in the vicinity of a flat-plate trailing edge have been carried out at NASA Glenn Research Center (Bridges, Brown and Bozak, 2014, Brown, 2015) in a facility validated for jet noise (Bridges and Brown, 2005; Brown and Bridges, 2006). Flow measurements for essentially the same geometries, but at a lower jet exit Mach number (M_a = 0.22), were carried out by Zaman et al (2013). We chose the configuration where the plate was located at 1.2 equivalent diameters from the jet centerline and 5.7 equivalent diameters downstream of the exit of an 8:1 rectangular nozzle, for jet exit acoustic Mach numbers $M_a=0.5,0.7,0.9$ as test cases for the theory. The arbitrary length scale D was taken to be an equivalent nozzle diameter defined by $\pi(D/2)^2$ =nozzle width $\times$ nozzle height with nozzle width=8 $\times$ nozzle height and was approximately equal to 2.12"inches in the experiments. Any `scrubbing noise' that may have resulted from the flow along the plate was deemed to be negligible for this configuration (Khavaran, Bozak and Brown, 2016). Recall that the source location is assumed to be at a large distance from edge and independent of its location on scale of the interaction, but not on the longer scale over which the turbulence and mean flow evolve. So the mean flow and turbulence properties must be recalibrated when changes in edge location occur on the latter scale.

Figure 6a shows a comparison of the normalized (by the jet exit velocity, U_J) mean velocity profile from the model (7.21) with velocity measurements at a very small distance downstream of the plate trailing edge carried out by Zaman et al (2013). Reynolds-averaged Navier-Stokes solutions for the test cases considered in this paper (Afsar et al 2017) show that the normalized mean velocity profiles for $M_a=0.5,0.7,0.9$ are similar to each other and to that measured by Zaman et al (2013) at M_a = 0.22. (There is a very slight miss-match in the transverse distance of the plate to the nozzle centerline between the Zaman et al (2013) experiment and the one where the acoustic data was taken, which accounts for the slightly higher velocity at $y_2/D_J=0$.) We therefore use the same normalized mean flow model for all jet exit velocities with the mean flow parameters for a best fit to the data. The data

shows that the mean velocity is small but not equal to zero at the interface. This can, in part, be attributed the turbulent mixing that that occurs upstream of the measuring station which, as noted above, was located down-stream of the trailing edge. But as pointed out by one of the referees, it could also be due to weakly non-linear velocity fluctuations, which causes the mean velocity to leave the trailing edge at different speeds above and below the plate. Hunt et al (2016) have recently shown that the mean speeds above and below the trailing edge can differ if the plate is at a small angle to the mean flow and similar effects could occur in the present case where it is aligned with the flow. However, the interface velocity is relatively small and is deemed to be insignificant relative to other uncertainties in the data comparisons.
Figure 6b compares the turbulent kinetic energy measurements from the same experiment to the amplitude $A(y_2, y_2)$ defined by (7.22)and(7.23) with the parameters A_0 and B_0 set equal to 0.011 and 0.022 respectively. The normalized turbulent kinetic energy profiles are also relatively independent of jet exit velocity and the models appear to be in reasonable agreement with the flow data. They are therefore used in the following noise predictions.

(a)

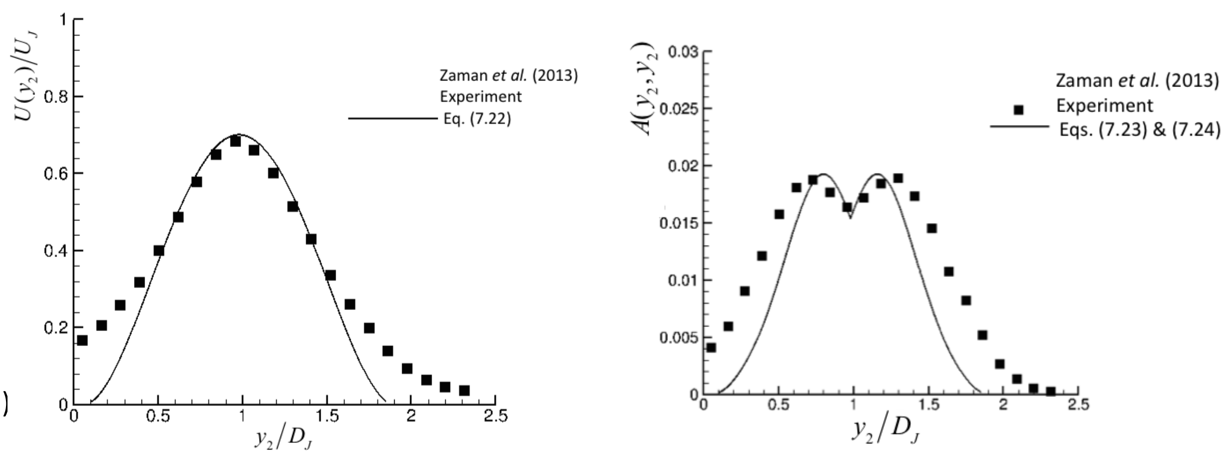

Figure 6 Comparison of (a) theoretical mean velocity profile and (b) mean flow shear calculated from equations (7.21) and (7.22) against experiments reported in Zaman *et al.* (2015). $(y_d, t_d) = (0.98, 1.85)$, $\kappa = 0.2$ and $(A_0, B_0) = (0.011, 0.022)$

Numerical results for the noise generated by jet-edge interaction are obtained by evaluating the formula (7.18) for the acoustic spectrum, with the double integrals being computed using a standard Simpson's method. The integrand in (7.18) vanishes outside of the support of the mean flow function (7.21) and the range of integration in this equation is therefore limited to the region where $U(y_2) \neq 0$.

Figures 8 through 10 show quantitative comparisons of measurements of the far-field pressure fluctuations' power spectral density per unit Strouhal number $= fD/U_J$, in dB scale $PSD = 10\log(4\pi I_\omega U_J / Dp_{ref}^2)$ (referenced to $p_{ref} = 20\mu pa$) taken by Brown (2015) with predictions obtained by inserting the spectrum (6.12) with $f = |\eta_2 / l_2| = |(y_2 - \tilde{y}_2)/l_2|$ into the composite RDT solution (7.18). Results are shown at observer locations directly below the plate $(\psi = -90^\circ)$ and several observer polar angles, θ, measured from the downstream jet axis. The experimental trailing-edge noise was educed by subtracting the noise measured in the corresponding free jet (i.e., in the absence of a plate) from the total measured noise. The parameters used in the predictions shown in figures 8-10 are $\tau_0 = 2.5$ and $(l_2, l_3) = (0.67, 0.25), \chi_0 = 1$. Setting the coefficient a_1 equal to 0.75 produces a turbulence correlation $\left\langle U_\perp\left(t - y_1/U(y_2), \mathbf{y}_T\right) U_\perp\left(t + \tilde{\tau} - y_1/U(y_2), \tilde{y}_2, y_2 + \eta\right)\right\rangle$ shown in figure 7 which exhibits the experimentally observed cusp behavior at zero spatial and temporal separations and the small but definite negative region at larger time delays.

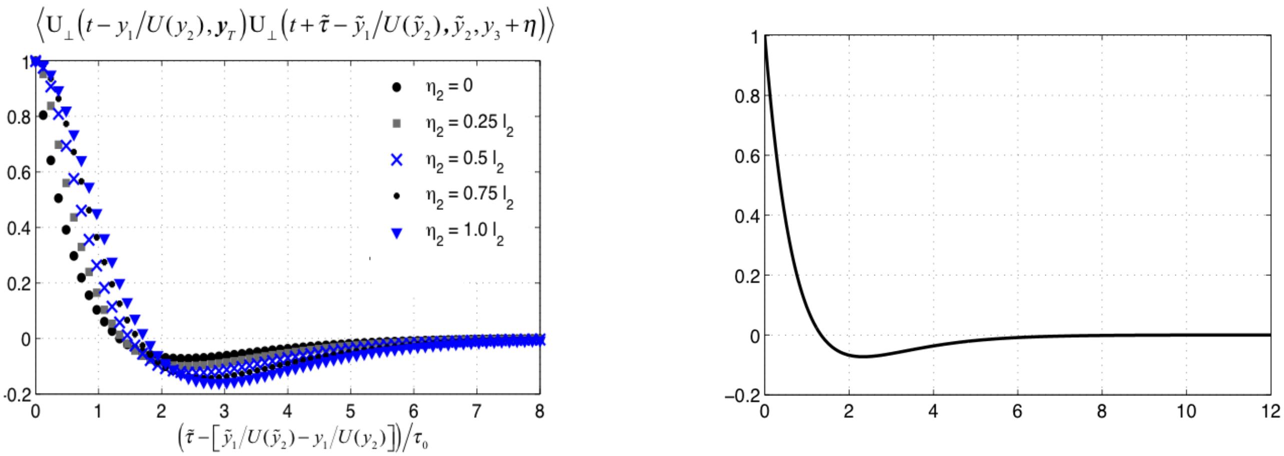

(a) (b)

Figure 7 Transverse turbulence correlation (6.7) at $\eta_3 = 0$ with parameters $\tau_0 = 2.5$, $(l_1, l_2) = (0.67, 0.25)$ and $a_1 = 0.75$ (a) fixed η_2 (b) $\eta_2 = 0$

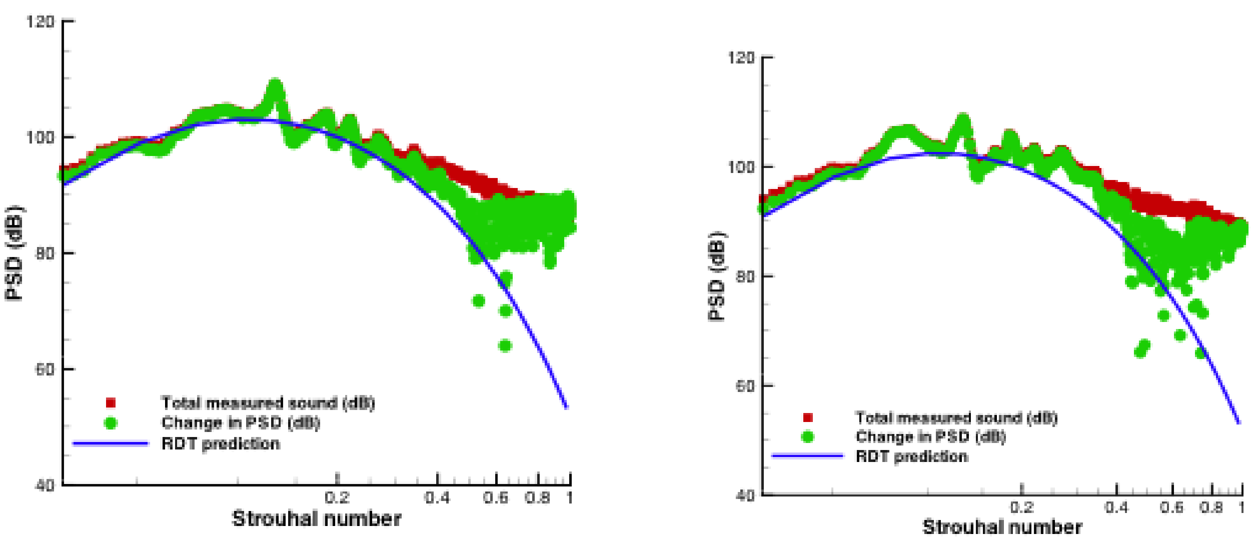

(a) -- (b).

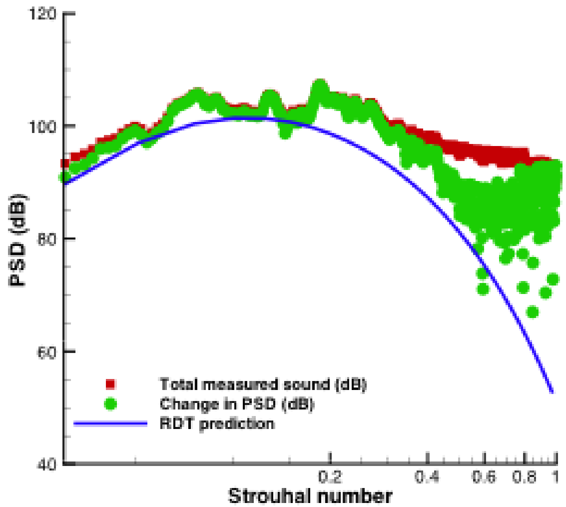

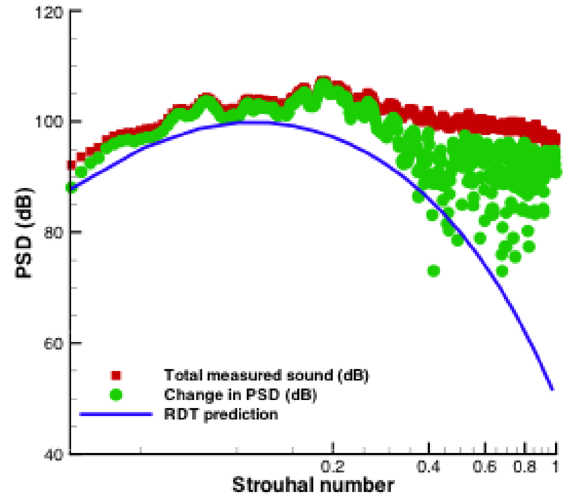

(c). (d).

Figure 8 Power Spectral Density (PSD) of the far-field pressure fluctuations at 100 equivalent diameters from nozzle exit (lossless in dB scale referenced to 20 μPa) as a function of Strouhal number, for $M_a = 0.9$. Predicted (solid line): Measured data below the plate at $\psi = -90^0$. (Total noise: Red; difference between the total noise and noise measured in the free jet: Green.) Plate trailing edge at $(x_d, y_d)/D = (5.7, 0.98)$ (a). $\theta = 90^0$; (b) $\theta = 75^0$ (c) $\theta = 60^0$ (d) $\theta = 45^0$

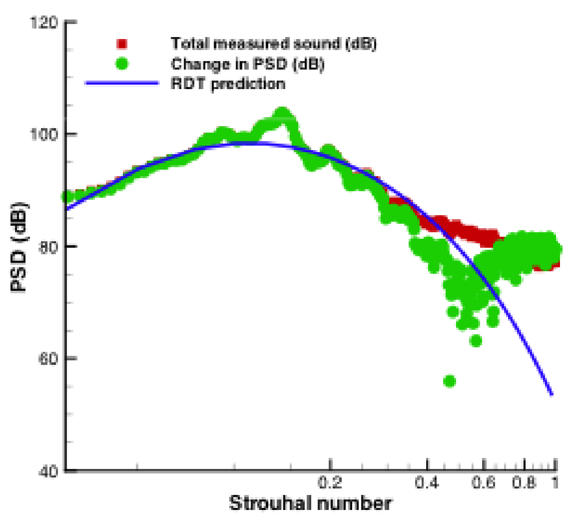

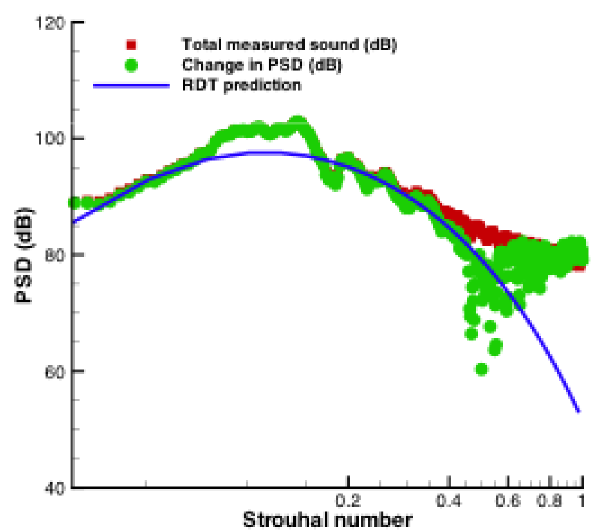

(a). (b)

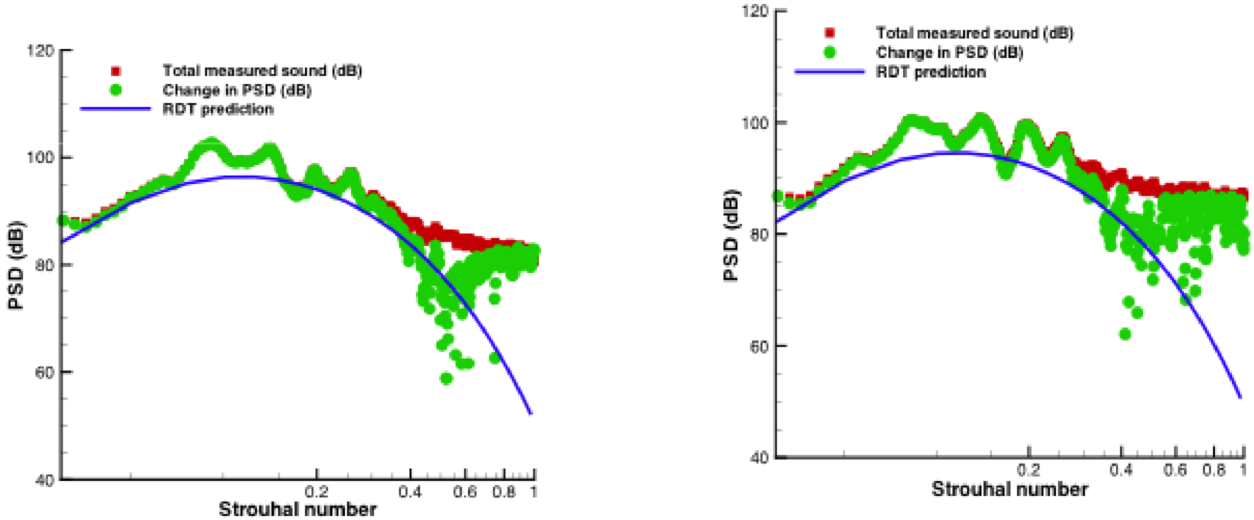

(c). (d).

Figure 9 Power Spectral Density (PSD) of the far-field pressure fluctuations at 100 equivalent diameters from nozzle exit (lossless in dB scale referenced to 20 μPa) as a function of Strouhal number, for $M_a = 0.7$. Predicted (solid line): Measured data below the plate at $\psi = -90^0$. (Total noise: Red; difference between the total noise and noise measured in the free jet: Green.) . Plate trailing edge at $(x_d, y_d)/D = (5.7, 0.98)$ (a). $\theta = 90^0$; (b) $\theta = 75^0$ (c) $\theta = 60^0$ (d) $\theta = 45^0$

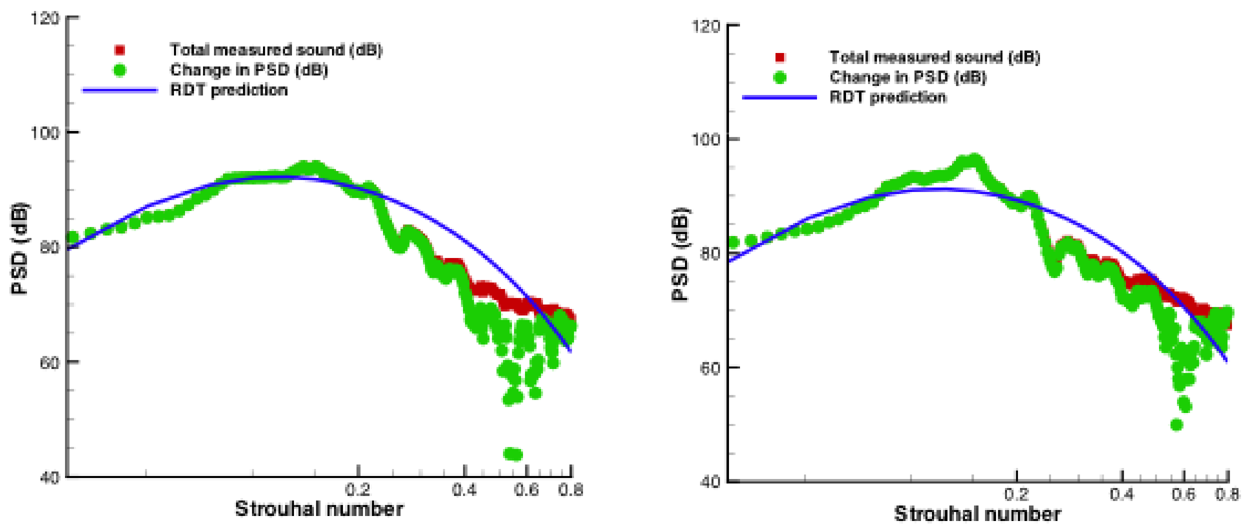

(a) (b)

.

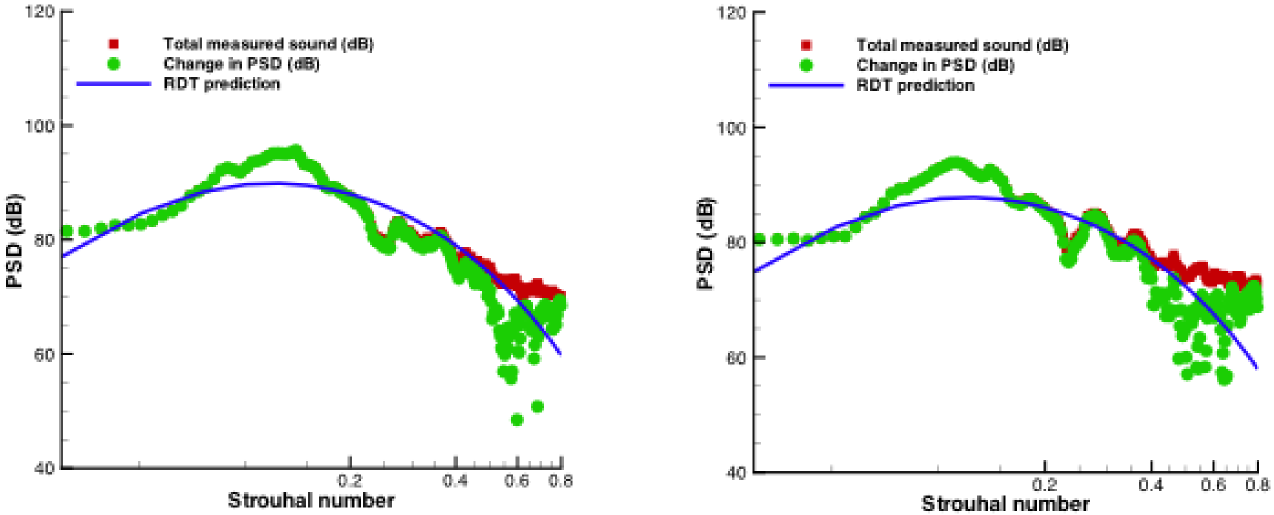

(c). (d).

Figure 10 Power Spectral Density (PSD) of the far-field pressure fluctuations at 100 equivalent diameters from nozzle exit (lossless in dB scale referenced to 20 μPa) as a function of Strouhal number, for $M_a = 0.5$. Predicted (solid line): Measured data below the plate at $\psi = -90^0$. (Total noise: Red; difference between the total noise and noise measured in the free jet: Green). Plate trailing edge at $(x_d, y_d)/D = (5.7, 0.98)$ (a). $\theta = 90^0$; (b) $\theta = 75^0$ (c) $\theta = 60^0$ (d) $\theta = 45^0$

The results for the downstream polar angles show that the RDT-based edge-noise predictions are now in much better agreement with the data than those given in Goldstein et al (2013) and Afsar *et al.* (2017). The agreement is now very good over the entire frequency range where the total measured noise (red symbols) is dominated by that generated by the jet-surface interaction alone (green symbols) for all jet exit Mach numbers at the downstream polar angles shown. The results of GAL were limited to St < 0.4 and Ma >= 0.7. The predictions shown in Figure 11 for upstream polar angles are also in very good agreement over the entire Mach number range.

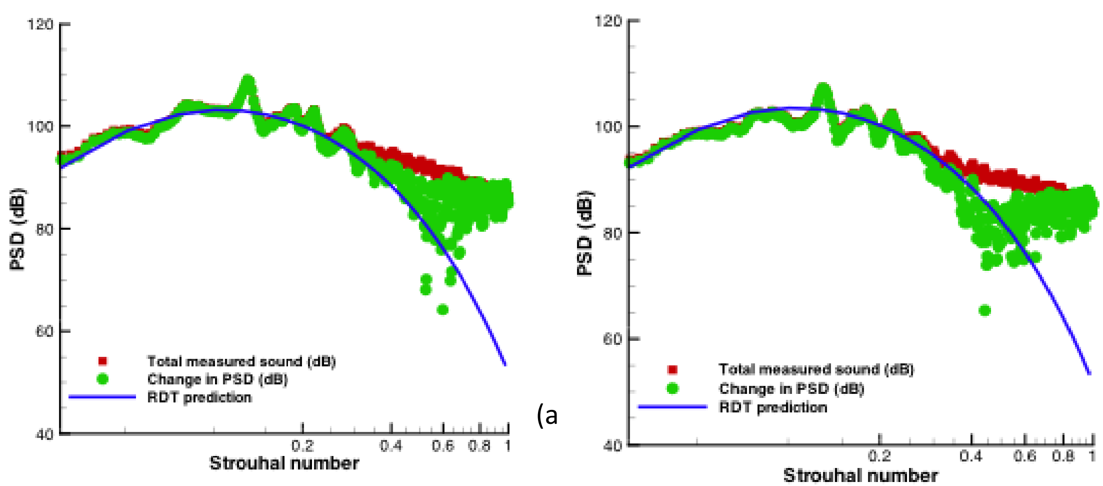

(a

(a) (b)

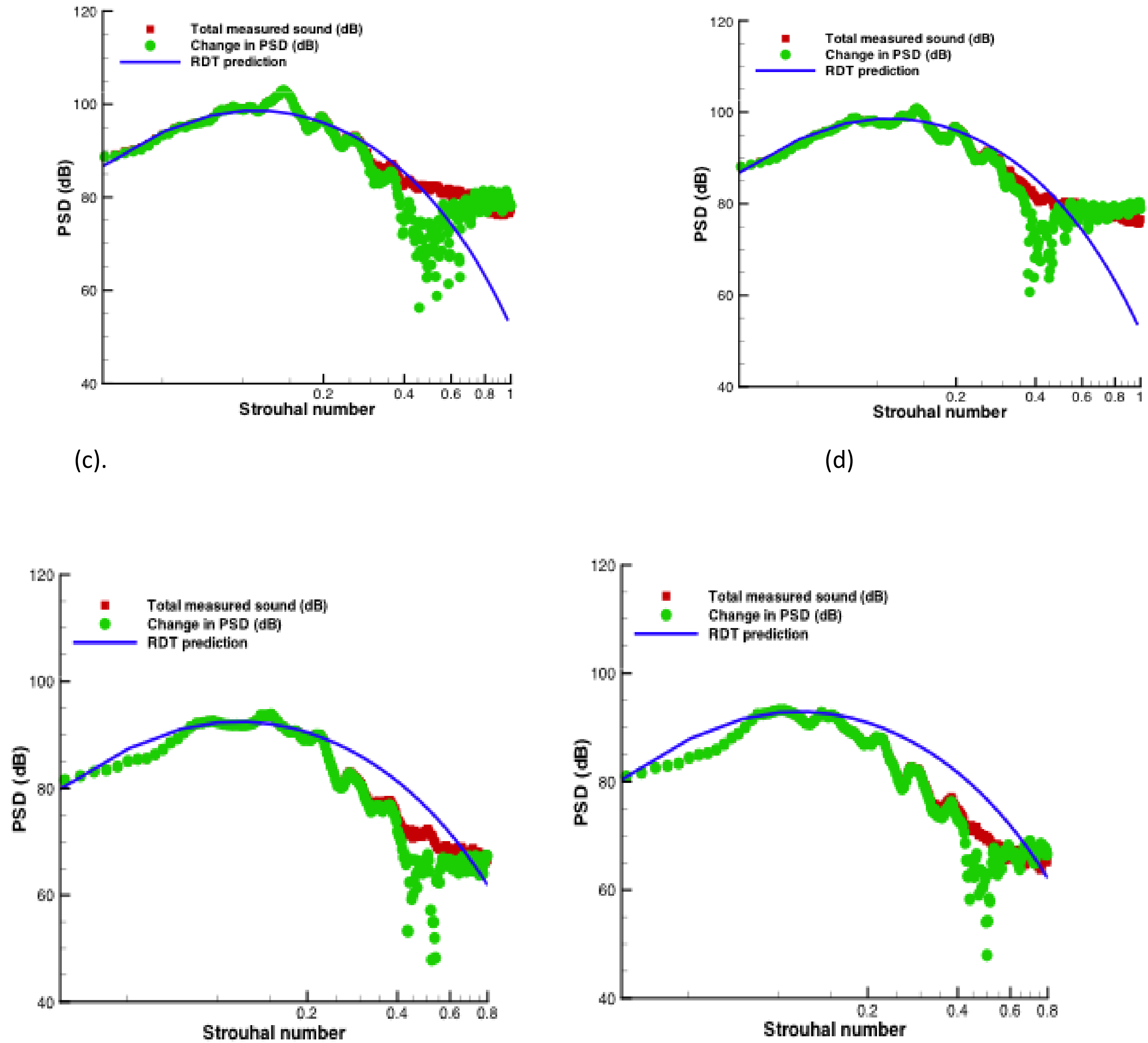

(c). (d)

(e) (f)

Figure 11. Power Spectral Density (PSD) of the far-field pressure fluctuations at 100 equivalent diameters from nozzle exit (lossless in dB scale referenced to 20 μPa) as a function of Strouhal number. Predicted (solid line): Measured data below the plate at $\psi = -90^0$. (Total noise: Red; difference between the total noise and noise measured in the free jet: Green.) For plate trailing edge at $(x_d, y_d)/D = (5.7, 0.98)$ (a). $M_a = 0.9, \theta = 95^0$; (b) $M_a = 0.9, \theta = 105^0$ (c) $M_a = 0.7, \theta = 95^0$ (d) $M_a = 0.7, \theta = 105^0$ (e) $M_a = 0.5, \theta = 95^0$; (f) $M_a = 0.5, \theta = 105^0$

Figure 12 is a comparison of the acoustic predictions obtained by inserting the present source function model (6.12) into the low frequency solution used in the GAL & Afsar et al 2017 for the parameter values used in figures 8-10. As expected , the present approach converges to the low frequency result at very low frequencies and, therefore, represents a much more robust mathematical model of trailing edge noise than either of the two previous studies since (for reasons indicated below (7.20)) it is now applicable to O(1) frequencies. And our numerical tests show that low frequency roll-off is now much less sensitive to the magnitude of the negative loop in the correlation function $\left\langle U_{\perp}\left(t-y_1/U\left(y_2\right),\boldsymbol{y}_T\right)U_{\perp}\left(t+\tilde{\tau}-y_1/U\left(y_2\right),\tilde{y}_2,y_2+\eta\right)\right\rangle$ than the Afsar et al 2017 model-although it is necessary to include this feature in the model in order for the transverse turbulence correlation to be physically realizable. In the present model the negative (anti-correlation) region enables the correct prediction of the absolute level of the very low frequency sound (i.e. for $St<0.1$) rather than the roll-off *per se.*

The improved predictions of the present result (relative to that obtained in GAL) is largely due to the $\exp\left(ik_{\infty}\int_0^{y_2}\sqrt{q\left(y\left|y_2\right.\right)}dy\right)$ factor in equation (7.19), which damps out the high frequencies and ,

therefore, increases the high frequency roll off, since the exponent $ik_{\infty}\int_0^{y_2}\sqrt{q\left(y\left|y_2\right.\right)}dy$ is always

negative. It accounts for the bending of the sound waves away from the downstream axis and, therefore, represents a kind of 'zone of silence'.

The present calculations are based on equation(6.4) which is obtained by using causality to interpret the singular integral (4.13) for the transverse particle displacement $\eta_{\perp}\left(\boldsymbol{y},\tau\right)$. But the causality condition results from an initial condition imposed in the distant past and, as argued in the introduction, the long-time solutions to the initial value problem are not necessarily relevant to the time-stationary turbulent flows being considered here. (Similar arguments can be found in Dowling, Ffowcs Williams and Goldstein; 1978 and Mani; 1976.) However, the singular integral in (4.13)will also be well defined if it is interpreted as a Cauchy principle value. The resulting formulas turn out to be more complicated than the present results and our computations (not shown here) indicate that the acoustic predictions based on these formulas do not differ significantly from the present results-at least in the low frequency limit where comparisons were carried out. Data comparisons, such as those given in this section, therefore, cannot be used to distinguish between the two.

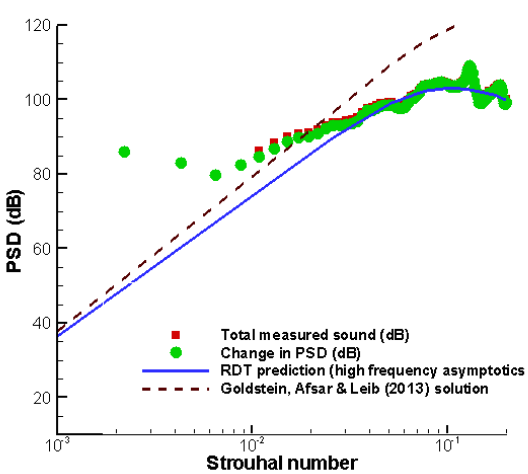

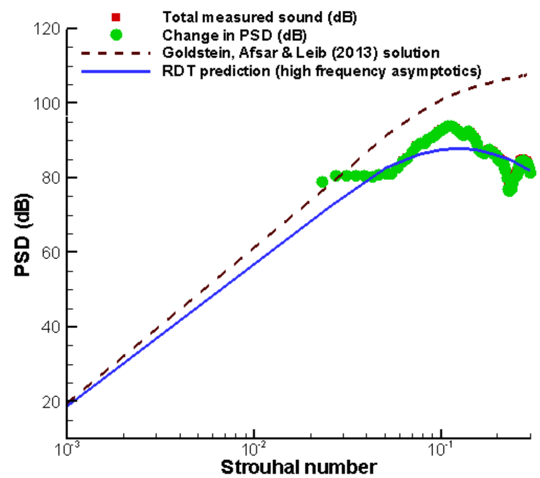

Figure 12. Convergence to the GAL solution. Same legend as Figs. 8-11. (a). $M_a = 0.9, \theta = 90^0$;
(b) $M_a = 0.5, \theta = 45^0$

Figures 8-10 show that that the predictions are better for larger polar angles (near ninety degrees) and higher Mach numbers as they were in GAL and Afsar et al 2017. The former is due to reduction in edge noise relative to the jet noise for shallow polar observation angles and the latter (the deterioration in prediction for $M_a < 0.5$ near $St \sim 0.1$) may be a particular feature of the experimental data (Bridges 2014) or may be associated with a change in the interference between the non-convecting jet noise and edge noise (Afsar et al 2017, p.202) at lower Mach numbers. There are four free parameters: (l_2, l_3, τ_0, a_1) that determine the source function S in the present model with all other parameters determined by matching to the turbulence or mean flow data, which makes the predictions much less empirical than those of GAL and Afsar et al 2017. No empirical coefficients would be required if there were experimental database for the transverse velocity correlation $\left\langle U_\perp\left(t - y_1/U(y_2), \boldsymbol{y}_T\right) U_\perp\left(t + \tilde{\tau} - y_1/U(y_2), \tilde{y}_2, y_2 + \eta\right)\right\rangle$. It could also be obtained computationally using LES which would be much less expensive than a jet noise simulation. The parameters could, in principle also be obtained by optimizing the agreement with the measured spectra.

8. Concluding remarks

This paper is based on the formal solutions (2.14)-(2.16) to the linearized Euler equations for transversely sheared mean flows which, like the Kovasznay results for the unsteady motion on uniform flows, involve two arbitrary convected quantities $\vartheta\left(\tau - y_1/U_{,}\boldsymbol{y}_T\right)$ and $\tilde{\omega}_c\left(\tau - y_1/U_{,}\boldsymbol{y}_T\right)$ that can be associated with the hydrodynamic component of the flow and can, therefore, be used to specify upstream boundary (i.e., initial) conditions for RDT problems that involve the interaction of turbulence with solid surfaces. This paper derives a new relation between these quantities and the physically measurable variables that is much simpler and more general than the one given in Goldstein et al (2013).

This relation was used to relate the source term S that appears in in a formula (7.2) for the noise generated by the interaction of a two-dimensional jet with a semi-infinite flat plate derived in Goldstein et al (2013) to the physically measurable second order velocity correlations in the jet. The result was combined with a modified high frequency solution to obtain a specific formula for the acoustic spectrum that applies over a broad range of frequencies. This result was then compared with experimental measurements carried out at Glenn Research Centre and excellent agreement was obtained. The general results can of course, be applied to many other RDT problems involving the interaction of turbulence with surfaces embedded in transversely sheared base flows or, more generally, in vortical base flows that asymptote to transversely sheared mean flows in the upstream region.

Acknowledgement

The authors would like to thank Drs. Khairul Zaman, James Bridges and Clifford Brown for providing their experimental data and their helpful comments. This work was also supported by the NASA Advanced Air Vehicles Program, Commercial Supersonic Technology Project. MZA would like to thank Strathclyde University for financial support from the Chancellor's Fellowship.

Appendix A. Green's function for 2-D base flow

Since $\bar{G}(\boldsymbol{y}_T \mid \boldsymbol{x}_T : \omega, k_1)$ can only depend on x_3 and y_3 in the combination $x_3 - y_3$, for the planer mean flow

$$U = U(y_2), \quad c = c(y_2) \tag{A.1}$$

the reduced Green's function

$$\hat{G}\left(y_2 \middle| x_2 : \omega, k_1, \hat{k}\right) \equiv \frac{1}{2\pi} \int_{-\infty}^{\infty} e^{i(y_3 - x_3)\hat{k}} \bar{G}(\boldsymbol{y}_T \mid \boldsymbol{x}_T : \omega, k_1) d(y_3 - x_3) \tag{A.2}$$

only depends on the indicated arguments and satisfies the reduced Rayleigh equation

$$\frac{d}{dy_2}\left\{\frac{c^2(y_2)}{\left[\omega - U(y_2)k_1\right]^2}\frac{d\hat{G}}{dy_2}\right\} + \left\{1 - \frac{c^2(y_2)}{\left[\omega - U(y_2)k_1\right]^2}\left(k_1^2 + k_3^2\right)\right\}\hat{G} = \frac{\delta(x_2 - y_2)}{(2\pi)^3}, \tag{A.3}$$

whose solution is given by

$$\hat{G}(y_2 \mid x_2) = \hat{G}(x_2 \mid y_2) = \frac{\hat{P}_{\pm}(y_2)\hat{P}_{\mp}(x_2)}{\Delta(k_1, k_3, \omega)} \quad \text{for } y_2 > / < x_2, \tag{A.4}$$

where $\hat{P}_{+}(y_2), \hat{P}_{-}(y_2)$ are the homogeneous solutions of (A.3) that exhibit appropriate boundary conditions at the outer/inner edges of the shear layer and, according to Abel's theorem,

$$\Delta(\omega, k_1, k_3) \equiv -\frac{(2\pi)^3 c^2\left[\hat{P}_{+}(y_2)\hat{P}_{-}'(y_2) - \hat{P}_{-}(y_2)\hat{P}_{+}'(y_2)\right]}{\left[\omega - U(y_2)k_1\right]^2} \tag{A.5}$$

depends on the normalization of $\hat{P}_{+}(y_2), \hat{P}_{-}(y_2)$ but is independent of y_2, which means that the reduced transverse velocity Green's function

$$\hat{G}_2\left(y_2 \middle| x_2 : \omega, k_1, k_3\right) = \frac{1}{2\pi} \int_{-\infty}^{\infty} e^{-ik_3((y_3 - x_3))} \bar{G}_2(\boldsymbol{y}_T \mid \boldsymbol{x}_T : \omega, k_1) d(y_3 - x_3), \tag{A.6}$$

where $\bar{G}_2(\boldsymbol{y}_T \mid \boldsymbol{x}_T : \omega, k_1)$ is defined by (4.9), only depends on the indicated argument and is given by

$$\hat{G}_2(y_2 \mid x_2) = \frac{1}{\left[ik_1 U(x_2) - i\omega\right]}\frac{\partial}{\partial x_2}\frac{\hat{P}_{\pm}(y_2)P_{\mp}(x_2)}{\Delta(k_1, k_3, \omega)} \quad \text{for } y_2 > / < x_2, \tag{A.7}$$

So the limit

$$\lim_{k_1\to\omega/U(y_2)}\Delta\left(k_1,k_3,\omega\right) \tag{A.8}$$

is expected to exist and be non-zero except at perhaps at a finite number of points, say $y_2 = y_2^{(n)}(\omega),$ for $n=1,2,...$ for any value of k_3,ω. This also shows that $\hat{G}_2\left(y_2\middle|x_2:\omega,\omega/U\left(y_2\right)k_3\right)$ and, therefore, $\bar{G}_2\left(\boldsymbol{y}_T\middle|\boldsymbol{x}_T:\omega,\omega/U\left(y_2\right)\right)$ must be continuous at $x_2=y_2$. Moreover it follows from the method of Frobenius that (A.3) possess two linearly independent solutions, say $\hat{P}_1\left(y_2\right),\hat{P}_2\left(y_2\right)$, that behave like

$$\hat{P}_1\left(y_2\right)=O\left(\left(\omega-k_1U\left(y_2\right)\right)^3\right)=O\left(\left(y_2-y_2^{(0)}\right)^3\right), \tag{A.9}$$

$$\hat{P}_2\left(y_2\right)=a+b\left(\omega-k_1U\left(y_2\right)\right)^2+c\hat{P}_1\left(y_2\right)\ln\left(\omega-k_1U\left(y_2\right)\right)+O\left(\left(y_2-y_2^{(0)}\right)^3\right), \tag{A.10}$$

as $y_2\to y_2^{(0)}$, where $y_2^{(0)}$ is a point where $U\left(y_2^{(0)}\right)=\omega/k_1$ and a,b,c are constants. So

$$\lim_{\substack{k_1\to\omega/U(y_2)\\ y_2=const.}}\left\{\hat{P}_+\left(y_2:k_1,k_3,\omega\right),\hat{P}_-\left(y_2:k_1,k_3,\omega\right)\right\}=$$

$$\lim_{\substack{y_2\to y_2^{(0)}\\ y_2^{(0)}=const.}}\left\{\hat{P}_+\left(y_2:\omega/U\left(y_2^{(0)}\right),k_3,\omega\right),\hat{P}_-\left(y_2:\omega/U\left(y_2^{(0)}\right),k_3,\omega\right)\right\} \tag{A.11}$$

is also expected to exist and be non-zero since $\hat{P}_+\left(y_2\right),\hat{P}_-\left(y_2\right)$ must be linear combinations of $\hat{P}_1\left(y_2\right),\hat{P}_2\left(y_2\right)$. It, therefore, follows from (A.2)and (A.4) that the limits

$$\bar{G}_0\left(\boldsymbol{y}_T\mid\boldsymbol{x}_T:\omega,\omega/U\left(\boldsymbol{y}_T\right)\right)\equiv\lim_{k_1\to\omega/U(\boldsymbol{y}_T)}\bar{G}_0\left(\boldsymbol{y}_T\mid\boldsymbol{x}_T:\omega,k_1\right) \tag{A.12}$$

and

$$\bar{G}_i\left(\boldsymbol{y}_T\mid\boldsymbol{x}_T:\omega,\omega/U\left(\boldsymbol{y}_T\right)\right)\equiv\lim_{k_1\to\omega/U(\boldsymbol{y}_T)}\bar{G}_i\left(\boldsymbol{y}_T\mid\boldsymbol{x}_T:\omega,k_1\right) \tag{A.13}$$

also exists and are non-zero everywhere except at the finite number of points where $\Delta\left(k_1,k_2,\omega\right)$ is equal to zero.

Appendix B. Behavior of transverse velocity at upstream infinity

When the mean flow is two dimensional the integral

$$I_i\equiv\int_{A_T}e^{i\omega x_1/U(\boldsymbol{y}_T)}\bar{G}_i\left(\boldsymbol{y}_T\mid\boldsymbol{x}_T:\omega,\omega/U\left(\boldsymbol{y}_T\right)\right)\bar{\Omega}_c\left(\boldsymbol{y}_T:\omega\right)d\boldsymbol{y}_T \tag{B.1}$$

on the right hand side of (4.3)can be written as

$$I_2(\boldsymbol{x}:\omega)=\int_{-\infty}^{\infty}\int_{y_0}^{\infty}e^{i\omega x_1/U(y_2)}\bar{G}_2(y_2,y_3\,|\,x_2,x_3:\omega,\omega/U(y_2))\bar{\Omega}_c(y_2,y_3:\omega)\,dy_2dy_3 \qquad \text{(B.2)}$$

where y_0 can be set to $-\infty$ if the cross sectional A_T is all of space and can be set to zero if the flow is bounded by an inner surface that extends from $y_1=-\infty$ to $y_1=+\infty$. Now suppose that

$$\bar{\Omega}_c(y_2,y_3:\omega)=O\left(\left[U'(y_2)\right]^3\right) \qquad \text{(B.3)}$$

whenever $U'(y_2)\to 0$. (We shall verify that $\bar{\Omega}_c(y_2,y_3:\omega)$ actually exhibits this behavior after the fact.) Then since $\bar{G}_2(y_2,y_3\,|\,x_2,x_3:\omega,\omega/U(y_2))$ is continuous at $y_2=x_2$ and $U^2(y_2)/U'(y_2)$ times the integrand and $U^2(y_2)/U'(y_2)$ times the derivative of this quantity are expected to vanish at the end points y_0,∞, (B.2)can be integrated by parts twice from y_0 to x_2 and from x_2 to ∞, to show that

$$I_2\equiv\frac{1}{i\omega x_1}\int_{-\infty}^{\infty}\int_{y_0}^{\infty}e^{i\omega x_1/U(y_2)}\frac{\partial}{\partial y_2}\left[\frac{U^2(y_2)}{U'(y_2)}\bar{G}_2(y_2,y_3\,|\,x_2,x_3:\omega,\omega/U(y_2))\bar{\Omega}_c(y_2,y_3:\omega)\right]dy_2dy_3$$

$$=-e^{i\omega x_1/U(x_2)}\left[\frac{U^2(x_2)}{\omega x_1U'(x_2)}\right]^2\int_{-\infty}^{\infty}\Delta\left[\frac{\partial}{\partial x_2}\bar{G}_2(x_2,y_3\,|\,x_2,x_3:\omega,\omega/U(x_2))\right]\bar{\Omega}_c(x_2,y_3:\omega)\,dy_3$$

$$-\frac{1}{(\omega x_1)^2}\int_{-\infty}^{\infty}\int_{y_0}^{\infty}e^{i\omega x_1/U(y_2)}\frac{\partial}{\partial y_2}\left\{\frac{U^2(y_2)}{U'(y_2)}\frac{\partial}{\partial y_2}\left[\frac{U^2(y_2)}{U'(y_2)}\bar{G}_2(y_2,y_3\,|\,x_2,x_3:\omega,\omega/U(y_2))\right.\right.$$

$$\left.\left.\times\bar{\Omega}_c(y_2,y_3:\omega)\right]\right\}dy_2dy_3 \qquad \text{(B.4)}$$

where the jump

$$\Delta\left[\frac{\partial}{\partial x_2}\bar{G}_{i2}(x_2,y_3\,|\,x_2,x_3:\omega,\omega/U(x_2))\right]\equiv\lim_{\varepsilon\to0}\left[\frac{\partial}{\partial y_2}\bar{G}_2(y_2,y_3\,|\,x_2,x_3:\omega,\omega/U(y_2))\Big|_{y_2=x_2+\varepsilon}\right.$$

$$\left.-\left[\frac{\partial}{\partial y_2}\bar{G}_2(y_2,y_3\,|\,x_2,x_3:\omega,\omega/U(y_2))\Big|_{y_2=x_2-\varepsilon}\right]\right] \qquad \text{(B.5)}$$

will, in general, be non –zero But this implies that

$$I_2 \to -e^{i\omega x_1/U(x_2)}\left[\frac{U^2(x_2)}{\omega x_1 U'(x_2)}\right]^2 \int_{-\infty}^{\infty} \Delta\left[\frac{\partial}{\partial x_2}\bar{G}_2\left(x_2, y_3 \mid x_2, x_3 : \omega, \omega / U(x_2)\right)\right]\bar{\Omega}_c\left(x_2, y_3 : \omega\right) dy_3 \quad \text{(B.6)}$$

as $x_1 \to -\infty$ since the method of stationary phase (Carrier, Krook and Pearson, 1966, p.274) (or continued integration by parts if there is no stationary phase point) can be used to show that that the last term(B.4) is $O\left(1/x_1^{5/2}\right)$ in this limit.

Appendix C. Upstream behavior of transverse particle displacement

We assume, for simplicity that there is a one-to-one mapping $\boldsymbol{y}_T \to \{\eta(\boldsymbol{y}_T), \varsigma(\boldsymbol{y}_T)\}$ of the rectangular coordinate system $\boldsymbol{y}_T$ into an orthogonal coordinate system $\{\eta, \varsigma\}$ such that $U = U(\eta)$ and introduce this into the integral in (4.13)to obtain

$$\int_{A_T} e^{i\omega x_1/U(\boldsymbol{y}_T)} \frac{\bar{G}_i\left(\boldsymbol{y}_T \mid \boldsymbol{x}_T : \omega, \omega / U(\boldsymbol{y}_T)\right)}{U(\boldsymbol{x}_T) - U(\boldsymbol{y}_T)} \bar{\Omega}_c\left(\boldsymbol{y}_T : \omega\right) d\boldsymbol{y}_T =$$

$$= \int_{C_T} \left[\int_{\eta_0}^{\infty} e^{i\omega x_1/U(\eta)} \frac{\bar{G}_i\left(\eta, \varsigma \mid: \boldsymbol{x}_T, \omega, \omega / U(\eta)\right)}{\left[U(\boldsymbol{x}_T) - U(\eta)\right]} \bar{\Omega}_c(\eta, \varsigma : \omega) \frac{\partial(y_2, y_3)}{\partial(\eta, \varsigma)} d\eta\right] d\varsigma$$

$$= \int_{-\infty}^{\infty} \int_{C_T} \left[\int_{\eta_0}^{\infty} e^{ikx_1} \delta\left(k - \omega / U(\eta)\right) \frac{k\bar{G}_i(\eta, \varsigma \mid: \boldsymbol{x}_T, \omega, k)}{\left[kU(\boldsymbol{x}_T) - \omega\right]} \bar{\Omega}_c(\eta, \varsigma : \omega) \frac{\partial(y_2, y_3)}{\partial(\eta, \varsigma)} d\eta\right] d\varsigma dk$$

$$\triangleq \lim_{n\to\infty} \lim_{\varepsilon \to 0} \int_{-\infty}^{\infty} \int_{C_T} \left[\int_{\eta_0}^{\infty} e^{ikx_1} \left(\frac{n}{\pi}\right)^{1/2} e^{-n\left[k - (\omega + i\varepsilon)/U(\eta)\right]^2} \frac{k\bar{G}_i(\eta, \varsigma \mid: \boldsymbol{x}_T, \omega + i\varepsilon, k)}{\left[kU(\boldsymbol{x}_T) - \omega - i\varepsilon\right]} \bar{\Omega}_c(\eta, \varsigma : \omega + i\varepsilon) \right.$$

$$\left. \times \frac{\partial(y_2, y_3)}{\partial(\eta, \varsigma)} d\eta\right] d\varsigma dk \quad \text{(C.1)}$$

where $\partial(y_2, y_3)/\partial(\eta, \varsigma)$ denotes the Jacobian of the transform $\boldsymbol{y}_T \to \{\eta, \varsigma\}$,we have represented the delta function by a delta sequence (see Lighthill, 1964 p.17) and have written $U(\eta) \equiv U(\boldsymbol{y}_T(\eta))$, $\bar{G}_i(\eta, \varsigma \mid: \boldsymbol{x}_T, \omega, \omega / U(\eta)) \equiv \bar{G}_i(\boldsymbol{y}_T(\eta, \varsigma) \mid: \boldsymbol{x}_T, \omega, \omega / U(\eta))$ etc. Then since $1/\left[kU(\boldsymbol{x}_T) - \omega - i\varepsilon\right]$ is the only term that becomes infinite on the real k-axis when $\varepsilon = 0$, the limit can be made explicit everywhere else in the n^th^ member of the sequence by setting $\varepsilon = 0$ there to obtain

$$\lim_{\varepsilon\to 0}\int_{-\infty}^{\infty}\int_{C_T}\left[\int_{\eta_0}^{\infty} e^{ikx_1}\left(\frac{n}{\pi}\right)^{1/2} e^{-n\left[k-(\omega+i\varepsilon)/U(\eta)\right]^2}\frac{k\bar{G}_i\left(\eta,\varsigma\,|\!:\boldsymbol{x}_T,\omega+i\varepsilon,k\right)}{\left[kU\left(\boldsymbol{x}_T\right)-\omega-i\varepsilon\right]}\bar{\Omega}_c\left(\eta,\varsigma:\omega+i\varepsilon\right)\right.$$

$$\left.\times\frac{\partial\left(y_2,y_3\right)}{\partial\left(\eta,\varsigma\right)}d\eta\right]d\varsigma dk$$

$$=\lim_{\varepsilon\to 0}\int_{-\infty}^{\infty}\int_{C_T}\left[\int_{\eta_0}^{\infty} e^{ikx_1}\left(\frac{n}{\pi}\right)^{1/2} e^{-n\left[k-\omega/U(\eta)\right]^2}\frac{k\bar{G}_i\left(\eta,\varsigma\,|\!:\boldsymbol{x}_T,\omega,k\right)}{\left[kU\left(\boldsymbol{x}_T\right)-\omega-i\varepsilon\right]}\bar{\Omega}_c\left(\eta,\varsigma:\omega\right)\frac{\partial\left(y_2,y_3\right)}{\partial\left(\eta,\varsigma\right)}d\eta\right]d\varsigma dk$$

The delta sequence limit can then be re-taken to show that the singular integral in (4.13) can be interpreted in the following sense

$$\int_{A_T} e^{i\omega x_1/U(y_T)}\frac{\bar{G}_i\left(\boldsymbol{y}_T\,|\,\boldsymbol{x}_T:\omega,\omega/U\left(\boldsymbol{y}_T\right)\right)}{U\left(\boldsymbol{x}_T\right)-U\left(\boldsymbol{y}_T\right)}\bar{\Omega}_c\left(\boldsymbol{y}_T:\omega\right)d\boldsymbol{y}_T \triangleq$$

$$=\frac{1}{U\left(\boldsymbol{x}_T\right)}\lim_{\bar{\varepsilon}\to 0}\int_{C_T}\left\{\int_{\eta_0}^{\infty} e^{i\omega x_1/U(\eta)}\frac{U'(\eta)H\left(\eta,\varsigma\,|\,\boldsymbol{x}_T:\omega\right)}{\left[U^{-1}(\eta)-U^{-1}\left(\boldsymbol{x}_T\right)-i\bar{\varepsilon}/\omega\right]U^2(\eta)}d\eta\right\}d\varsigma \qquad \text{(C.2)}$$

where we have put $\bar{\varepsilon}\equiv\varepsilon/U\left(\boldsymbol{x}_T\right)$ and

$$H\left(\eta,\varsigma\,|\,\boldsymbol{x}_T:\omega\right)\equiv\frac{U(\eta)\bar{G}_i\left(\eta,\varsigma\,|\!:\boldsymbol{x}_T,\omega,\omega/U(\eta)\right)}{U'(\eta)}\bar{\Omega}_c\left(\eta,\varsigma:\omega\right)\frac{\partial\left(y_2,y_3\right)}{\partial\left(\eta,\varsigma\right)} \qquad \text{(C.3)}$$

But, as indicated in the introduction, our interest here is in the upstream behavior of the solutions as $x_1\to-\infty$. To this end we suppose, for definiteness, that the mean velocity profile has a single maximum, at say $\eta=\eta_{\max}$, that $U=0$ at the end points η_0,∞ and that

$$\bar{\Omega}_c\left(y_2,y_3:\omega\right)=O\left(\left[U'\left(y_2\right)\right]^2\right)\ \text{ when } U'\left(y_2\right)\to 0 \qquad \text{(C.4)}$$

(We shall verify that $\bar{\Omega}_c\left(y_2,y_3:\omega\right)$ actually exhibits this behavior after the fact.) Adding and subtracting terms to the particle displacement integral (C.1) then shows that

$$\int_{A_T} e^{i\omega x_1/U(y_T)}\frac{\bar{G}_i\left(\boldsymbol{y}_T\,|\,\boldsymbol{x}_T:\omega,\omega/U\left(\boldsymbol{y}_T\right)\right)}{U\left(\boldsymbol{x}_T\right)-U\left(\boldsymbol{y}_T\right)}\bar{\Omega}_c\left(\boldsymbol{y}_T:\omega\right)d\boldsymbol{y}_T =$$

$$=\frac{1}{U\left(\boldsymbol{x}_T\right)}\int_{C_T}\left\{\int_{\eta_0}^{\eta_{\max}} e^{i\omega x_1/U(\eta)}\frac{U'(\eta)\left[H\left(\eta,\varsigma\,|\,\boldsymbol{x}_T:\omega\right)-H\left(\bar{\eta}_1,\varsigma\,|\,\boldsymbol{x}_T:\omega\right)\right]}{\left[U^{-1}(\eta)-U^{-1}\left(\boldsymbol{x}_T\right)\right]U^2(\eta)}d\eta+\right.$$

$$\int_{\eta_{\max}}^{\infty} e^{i\omega x_1/U(\eta)} \frac{U'(\eta)\left[H(\eta,\varsigma\,|\,\boldsymbol{x}_T:\omega)-H(\bar{\eta}_2,\varsigma\,|\,\boldsymbol{x}_T:\omega)\right]}{\left[U^{-1}(\eta)-U^{-1}(\boldsymbol{x}_T)\right]U^2(\eta)}d\eta\Bigg\}d\varsigma$$

$$-\frac{1}{U(\boldsymbol{x}_T)}\int_{C_T}\left[H(\bar{\eta}_1,\varsigma\,|\,\boldsymbol{x}_T:\omega)-H(\bar{\eta}_2,\varsigma\,|\,\boldsymbol{x}_T:\omega)\right]d\varsigma\left\{\lim_{\bar{\varepsilon}\to 0}\int_a^{\infty}\frac{e^{i\omega x_1/U}}{\left[U^{-1}-U^{-1}(\boldsymbol{x}_T)-i\bar{\varepsilon}/\omega\right]}d\left(\frac{1}{U}\right)\right\} \qquad \text{(C.5)}$$

where $a \equiv 1/U(\eta_{\max})$, and $\bar{\eta}_j$ for $j=1,2$ are the roots of $U(\bar{\eta}_j)=U(\boldsymbol{x}_T)$ with $U'(\bar{\eta}_1)<0$.

But dividing the range of integration into two parts, changing integration variables and noting that the final contour integral must be closed in the lower half plane for $x_1<0$ shows that

$$\lim_{\bar{\varepsilon}\to 0}\int_a^{\infty}\frac{e^{i\omega x_1\left[U^{-1}-U^{-1}(\boldsymbol{x}_T)\right]}}{\left[U^{-1}-U^{-1}(\boldsymbol{x}_T)-i\bar{\varepsilon}/\omega\right]}d\left(\frac{1}{U}\right)=\lim_{\bar{\varepsilon}\to 0}\left\{\int_{-b(\boldsymbol{x}_T)\omega x_1}^{\infty\operatorname{sgn}\omega}\frac{e^{it}}{t-i\bar{\varepsilon}x_1}dt+e^{-i\omega x_1/U(\boldsymbol{x}_T)}\int_{-\infty\operatorname{sgn}\omega}^{\infty\operatorname{sgn}\omega}\frac{e^{i\tau x_1}}{\tau-i\bar{\varepsilon}}d\tau\right\}=$$

$$\lim_{\bar{\varepsilon}\to 0}\left\{\int_{-b(\boldsymbol{x}_T)\omega x_1}^{\infty\operatorname{sgn}\omega}\frac{e^{it}}{t-i\bar{\varepsilon}x_1}dt+e^{-i\omega x_1/U(\boldsymbol{x}_T)}\operatorname{sgn}\omega\int_{-\infty}^{\infty}\frac{e^{i\tau x_1}}{\tau-i\bar{\varepsilon}}d\tau\right\}\to 0, \qquad \text{(C.6)}$$

as $x_1\to-\infty$

where $b(\boldsymbol{x}_T)\equiv\left[U(\boldsymbol{x}_T)\right]^{-1}-a>0$. And since the integrands of the inner integrals in the first term on the right hand side of (C.5) are now finite at $\boldsymbol{y}_T=\boldsymbol{x}_T$, the first of these can be integrated by parts from η_0 to $\bar{\eta}_1$ and from $\bar{\eta}_1$ to $\eta_{\max}$ to obtain

$$\frac{1}{U(\boldsymbol{x}_T)}\left\{\int_{\eta_0}^{\eta_{\max}} e^{i\omega x_1/U(\eta)}\frac{U'(\eta)\left[H(\eta,\varsigma\,|\,\boldsymbol{x}_T:\omega)-H(\bar{\eta}_1,\varsigma\,|\,\boldsymbol{x}_T:\omega)\right]}{\left[U^{-1}(\eta)-U^{-1}(\boldsymbol{x}_T)\right]U^2(\eta)}d\eta\right.$$

$$=-\frac{1}{i\omega x_1}e^{i\omega x_1/U(\bar{\eta}_1)}\Delta\left[\frac{\partial\bar{G}_2(\eta,\varsigma\,|\!:\boldsymbol{x}_T,\omega,\omega/U(\eta))}{\partial\eta}\right]\Bigg|_{\eta=\bar{\eta}_1}\left\{\frac{\bar{\Omega}_c(\eta,\varsigma:\omega)\dfrac{\partial(y_2,y_3)}{\partial(\eta,\varsigma)}}{\left[U'(\eta)\right]^2}\right\}_{\eta=\bar{\eta}_1}$$

$$-\frac{1}{i\omega x_1}\int_{\eta_0}^{\eta_{\max}} e^{i\omega x_1/U(\eta)}\frac{\partial}{\partial\eta}\left\{\frac{\left[H(\eta,\varsigma\,|\,\boldsymbol{x}_T:\omega)-H(\bar{\eta}_1,\varsigma\,|\,\boldsymbol{x}_T:\omega)\right]}{\left[U(\boldsymbol{x}_T)-U(\eta)\right]U(\eta)}\right\}d\eta \qquad \text{(C.7)}$$

where $\Delta\left[\partial\bar{G}_2\left(\eta,\varsigma\,|: \boldsymbol{x}_T,\omega,\omega/U(\eta)\right)/\partial\eta\right]\Big|_{\eta=\bar{\eta}_1}$ denotes the jump in $\partial\bar{G}_2\left(\eta,\varsigma\,|: \boldsymbol{x}_T,\omega,\omega/U(\eta)\right)/\partial\eta$ at $\eta=\bar{\eta}_1$ while the second of these can be integrated by parts from $\eta_{\max}$ to $\bar{\eta}_2$ and from $\bar{\eta}_2$ to ∞, to obtain a similar result and thereby show that this term is $O(1/x_1)$ as $x_1\to-\infty$, and, therefore, that $\bar{\eta}_\perp$ satisfies (4.14).

References

Afsar, M.Z., Leib, S.J. and Bozak, R.F., ' Effect of de-correlating turbulence on the low frequency decay of jet-surface interaction noise in sub-sonic unheated air jets using a CFD-based approach,' Journal of Sound and Vibration, Vol. 386, No. 6, pp. 177-207, 2017.

Afsar, M. Z., Sescu, A. & Leib,2016, S. J. Predictive capability of low frequency jet noise using an asymptotic theory for the adjoint vector Green's function in non-parallel flow. AIAA Aero-acoustics 2016. (AIAA 2016-2804).

Ayton, L.J., Gill, J. and Peak, N, 2016, 'The importance of the unsteady Kutta condition when modelling gust-aerofoil interaction, Journal of Sound and Vibration, Vol. 378, pp. 28-37.

Batchelor, G.K. and Proudman, I., 1954, The effect of rapid distortion of a fluid in turbulent motion, Quarterly Journal of Mechanics and Applied Mathematics, Vol. 7, No. 1 pp. 83 – 103.

Bers, A. 1975 Linear waves and instabilities. *In Plasma Physics* (eds. C. Dewitt & J. Perraud), pp. 113-216. Gordon & Breach.

Bridges, J., 2014, Noise from Aft Deck Exhaust Nozzles—Differences in Experimental Embodiments *52nd AIAA Aerospace Sciences Meeting – 13-17 January 2014, Nat'l Harbor, MD*

Bridges, J., Brown, C.A. and Bozak, R., 'Experiments on Exhaust of Tightly Integrated Propulsion Systems,' AIAA-2014-2904.

Bridges, J. and Brown, C.A. "Validation of the small hot jet rig for jet noise research," AIAA Paper 2005-2846, 2005.

Briggs, R. J. 1964 *Electron Stream Interaction with Plasmas.* MIT Press

Brinkman, K. W. & Walker, J. D. A., 2001, Instabilities in a viscous flow driven by streamwise vortices, J. Fluid Mech., **432**, pp. 127-166

Brown, S.N. and Daniels, P.G. 1975, On the viscous flow about the trailing edge of a rapidly oscillating plate, Journal of Fluid Mechanics, Vol. 67 , Issue 4 , pp. 743-761

Brown, C. , 2012 Jet-Surface Interaction Test: Far-Field Noise Results, ASME Paper GT2012-69639.

Brown, C.A. and Bridges, J., 2006, Small hot jet acoustic rig validation, NASA-TM-2006-214234.

Brown, Clifford A., 2015, An Empirical Jet-Surface Interaction Noise Model with Temperature and Nozzle Aspect Ratio Effects, *53rd AIAA Aerospace Sciences Meeting*.

Cassel & Conlisk, 2014, Unsteady separation in vortex induced boundary layers, Proc. Roy Soc. Vol. 372 No. 2020, 20130348

Chinaud, M., Rouchon, J.F., Duhayon, E., Scheller, J. Cazin, S., Marchal, M. and Braza, M., 2014, 'Trailing-edge dynamics and morphing of a deformable flat plate at high Reynolds number by time-resolved PIV,' Journal of Fluids and Structures, Vol. 47. pp. 41-54.

Cowley, 2001, Laminar boundary layer theory: A 20th century paradox?, Proc. ICTM 2000, Chicago, IL, Aug.-Sept 2000, , pp.389-411, Dordrect, The Netherlands: Kluwer

Crighton, D.G., 'The Kutta condition in unsteady flow,' 1985, Annual Review of Fluid Mechanics, Vol. 17, pp. 411-445.

Dowling, A. P., Ffowcs Williams J. E. & Goldstein, M. E. 1978, Sound propagation in a moving stream, Phil. Trans. R. Soc. London, A288 pp321-34940, 657-670

Drazin, P. G., Reid, W. H., 1981, Hydrodynamic Stability, Cambridge University Press, Cambridge UK

Goldstein, M.E., 1978a, Unsteady vortical and entropic distortions of potential flows round arbitrary obstacles, J. Fluid Mech. Vol.89, pp. 433-468

Goldstein, M.E., 1978b, Characteristics of the unsteady motion on transversely sheared mean Flows, J. Fluid Mech. Vol.84, part 2, pp. 305-329 Goldstein, M.E., 1979a, turbulence generated by entropy fluctuation with non-uniform mean flows, J. Fluid Mech. Vol. 93, part 2 pp. 209-224

Goldstein, M.E., 1979b, Scattering and distortion of the unsteady motion on transversely sheared mean Flows, J. Fluid Mech. Vol.91, part 4, pp. 601-632

Goldstein, M.E., 2005, On Identifying the true sources of aerodynamic sound , J. Fluid Mech. Vol. 526, pp. 337-347

Goldstein, M.E., 2009, A theoretical basis for identifying the sound sources in a turbulent flow, international journal of Aeroacoustics.Vol.8 no. 4, pp. 283-300

Goldstein, M.E., Afsar, M. Z. and Leib, 2013 a, Non-homogeneous rapid distortion theory on transversely sheared mean flows, J. Fluid Mech. Vol.736, pp. 532-569

Goldstein, M.E., Afsar, M. Z. and Leib, 2013 b, Structure of Small Amplitude Motion on Transversely Sheared Mean Flows, NASA/TM-2013-217862

Hunt, J. C. R. 1973 A theory of turbulent flow around two dimensional bluff bodies J. Fluid Mech. Vol. 61, pp. 625-706

Hunt, J.C.R., Ishihara, T. Szubert, D., Asproulias, I., Hoarau, Y. and Braza, M. 2016. Turbulence Near Interfaces—Modelling and Simulations, pp 283-292. Advances in Fluid-Structure Interaction. Updated contributions reflecting new findings presented at the ERCOFTAC Symposium on Unsteady Separation in Fluid-Structure Interaction, 17-21 June 2013, St John Resort, Mykonos, Greece. Springer Publications

Khavaran, A., Bozak, R.F. and Brown, C.A., 'Jet Surface Interaction Noise in a Planar Exhaust,' AIAA-2016-2863, 2016.

Kovasznay, L. S. G., 1953, Turbulence in supersonic flow, J. Aero Sci. 20, issue number 10pp. 657-674.

Leib, S.J. and Goldstein, M.E., 2011 "Hybrid Source Model for Predicting High-Speed Jet Noise," *AIAA Journal*, Vol. 49, No. 7

Lighthill, M. J. 1964 Fourier Analysis and Generalized Functions, Cambridge University Press

Mani, R. 1976, Influence of jet flow on jet noise, *Journal of Fluid Mech.* 173 pp. 753-793

Livescu, D. and Madnia, C.K. 2004, Small scale structure of homogenious turbulent shear flow phys. Fluids vol. 16, no.8 pp.2864-28787

Moffatt, H. K. (1967). Interaction of turbulence with strong wind shear, in Colloquium on Atmospheric Turbulence and Radio Wave Propagation, Edited by A. M. Yaglom and V. I. Tatarski (Nauka, Moscow, 1967), 139–156.

Möhring, W., 1976 Über Schallwellen in Scherströmungen, Fortschritte der Akustik. DAGA 76 VDI pp.543-546

Moore, F. K., 1954, 'Unsteady oblique interaction of a shock wave with a plane disturbance,'

NACS Tech. Rep. 2879.

Morse, P. M. and Feshbach, H., 1953, Methods of Theoretical Physics, McGraw-Hill Book Company

Orr, W. (1907), The stability and instability of the steady motions of a perfect liquid and of a viscous liquid, Proc. Roy. Irish Acad., A 27, 9-68 and 69-138

Ribner, H. S., 1953, 'Convection of a pattern of vorticity through a shock wave, ' NACA Tech.

Rep. 1164.

Sears, W.R., 1941, Some aspects of non-stationary airfoil theory and its practical application, J. Aero. Sci. vol. 83, p. 104

Tam, C. K.W. & Auriault, L. 1998, mean flow refraction effects on sound radiated from localized sources

Xie, Z., Karimi, M. & Girimaji, S. S. 2017, Small perturbation evolution in compressible Poiseulle flow-velocity interactions and obliqueness effects, *Journal of Fluid Mech.* 814 pp. 249-276

Taylor, G.I., 1935, Turbulence in a contracting stream, Z. Angew. Math. Mech., Vol 15, pp.91-96.

Weiner, N. 1938, The use of statistical theory to study turbulence, Proc.5th Int. Congress Appl. Mech. P.356-360

Zaman, K.; Brown, C. A.; Bridges, J. E., 2013, Interaction of a Rectangular Jet with a Flat-plate placed parallel to the Flow AIAA-2013-2184. (NASA/TM-2013-217879 (E-18684), 2013.